Quasi 2D-Ising-type Magnetic Critical Behavior in Trigonal $Cr_{1.27}Te_2$

Anirban Goswami[1], Nicholas Ng[2,3], Emmanuel Yakubu[1], Gregory Bassen[2,3] and Samaresh Guchhait[1*]

1. Department of Physics and Astronomy, Howard University, Washington, DC 20059, USA
2. Department of Chemistry, The Johns Hopkins University, Baltimore, MD 21218, USA
3. Institute for Quantum Matter, The William H. Miller III Department of Physics and Astronomy, The Johns Hopkins University, Baltimore, MD 21218, USA

Abstract

Single crystal $Cr_{1.27}Te_2$ samples were synthesized by chemical vapor transport method. Single crystal x-ray diffraction studies show trigonal crystal structure with $P\bar{3}m1$ symmetry space group. We then systematically investigate magnetic properties and critical behaviors of single crystal $Cr_{1.27}Te_2$ around its paramagnetic-to-ferromagnetic phase transition. The Arrott plot indicates a second order magnetic phase transition. We estimate critical exponents $\beta = 0.2631 \pm 0.002$, $\gamma = 1.2314 \pm 0.007$, and $T_C = 168.48 \pm 0.031$ K by Kouvel-Fisher method. We also estimate other critical exponents $\delta = 5.31 \pm 0.004$ by analyzing the critical isotherm at $T_C = 168.5$ K. We further verify the accuracy of our estimated critical exponents by the scaling analysis. Further analysis suggests that $Cr_{1.27}Te_2$ can be best described as a quasi-2D Ising magnetic system.

I. Introduction

Magnetic materials have gained lot of interests in the scientific and technology community. Magnetic materials are interesting because of richness of their fundamental physics and many technological applications depending on their properties. Now-a-days there are lots of interest in two-dimensional magnetic materials after the discovery of intrinsic magnetism in two-dimensional CrI_3 [1]. Besides, chromium and telluride based binary phases have received significant interests due to the existence of many magnetic phases. Cr-Te phase diagram has several stable binary phases, and some of these magnetic phases are predicted to be layered[2–5]. G. Chattopadhyay investigated the phase diagram of Cr_xTe_y compositions in-detail[5]. Reported stable binary Cr-Te phases include trigonal $Cr_{0.62}Te$[6], hexagonal CrTe[7], trigonal $CrTe_2$[8–10], trigonal Cr_2Te_3[11–13], monoclinic Cr_3Te_4[14,15], hexagonal $Cr_{1-x}Te$ ($x < 0.1$) [16], trigonal & monoclinic phases of Cr_5Te_8[17–20] and hexagonal Cr_5Te_6[21]. Recently, some layered room temperature magnetic Cr_xTe_y phases are (theoretically) predicted.

Binary chromium tellurides $Cr_{1-x}Te$ are ferromagnetic with Curie temperature T_C varies between 170–360 K depending on their Cr content[3,16]. There are alternating stacks of Cr-full and Cr-deficient layers along the *c*-axis in these compounds. The magnetic properties of these compounds are mainly driven by the interlayer coupling and the electron-correlation effect. Chromium content in these compounds plays the vital role in determining its crystal structure, nature of the magnetic interaction, Curie temperature etc.

Neutron diffraction studies of several Cr-Te compounds were performed in 1960s to determine the magnitude and orientation of its magnetic moments. The electronic band structure calculations were performed on CrTe, Cr_2Te_3, and Cr_3Te_4 phases[22], which suggest that Cr $3d_{z2}$ orbitals along the crystallographic *c*-direction overlap strongly due to relatively smaller nearest neighbor Cr–Cr distance. Moreover, heat capacity[23], reflectivity spectra[24], magnetic anisotropy[25], electronic structure[16,22], soft x-ray magnetic circular dichroism[26] studies have been reported on several Cr_xTe_y compounds before.

Here we report synthesis, characterization, and critical behavior studies of single crystal $Cr_{1.27}Te_2$. Singe crystal samples are synthesized by chemical vapor transport (CVT). Phase of our synthesized crystals are characterized by single crystal x-ray diffraction (XRD) technique and determined to have a chemical formula of $Cr_{1.27}Te_2$ with a trigonal phase and space group *P*-3*m*1. Previously, Neel-type skyrmions are observed in self-intercalated $Cr_{1.3}Te_2$ crystals which are synthesized by flux-zone growth[27]. Our synthesized system is closely related to the reported 1*T*-$CrTe_2$ phase (details later). Both bulk and epitaxially grown 1*T*-$CrTe_2$ samples have been reported before. Bulk metastable $CrTe_2$ crystals are synthesized by oxidizing $KCrTe_2$ crystals[10]. However, this process leaves some K atoms within these crystals. Previously, magnetic, heat capacity, transport, and magnetic force microscopy studies are performed on these bulk crystals, and these samples are found to have a Curie temperature ~315 K[10,28]. Magneto-transport studies are also performed on exfoliated ultra-thin films, and they are found to have anisotropic magnetoresistance[9]. 1*T*-CrT_2 films with different thickness are also grown by chemical vapor deposition and thickness dependent Curie temperature is observed in these samples[29]. Thin film $CrTe_2$/ bilayer graphene/ SiC heterostructures are grown by molecular beam epitaxy (MBE) and studied by x-ray magnetic circular dichroism. These samples have a Curie temperature ~300 K[9]. Epitaxially grown $CrTe_2/ZrTe_2$ samples also show anomalous Hall effects[30]. Moreover, first-principal calculations show presence of non-collinear magnetic structure in $CrTe_2$[8]. However, there is no report on critical behavior study in this material.

Our goal here is to study the nature of the magnetic phase transition in single crystal $Cr_{1.27}Te_2$ system. A better knowledge of this phase transition will also help us to understand its thermodynamic properties and explore possible applications of this material[27,31]. Here we estimate the critical exponents around its paramagnetic-to-ferromagnetic (PM-FM) phase transition by analyzing its isothermal magnetizations. Previously, critical behavior studies have been reported on other binary Cr-Te phases, such as Cr_4Te_5[32], Cr_3Te_4[33], Cr_5Te_8[18,19], Cr_5Te_6[34], etc. To the best of our knowledge, there is no report of critical behavior study on $Cr_{1.27}Te_2$ or $CrTe_2$ phases.

In this paper, we study magnetic critical behavior of $Cr_{1.27}Te_2$ crystal by modified Arrott plot (MAP), Kouvel-Fisher (KF) plot, and critical isotherm analysis. Through our critical analysis we

estimate critical exponents $\beta = 0.2631 \pm 0.002$, $\gamma = 1.2314 \pm 0.007$, $\delta = 5.31 \pm 0.004$ and $T_C = 168.48 \pm 0.031$ K. We then use the scaling analysis to verify the accuracy of our estimated critical exponents, followed by the renormalization-group-theory analysis to estimate its universality class. $Cr_{1.27}Te_2$ is a complex system with multiple interactions between its constituent atoms[8]. Nevertheless, our critical analysis shows that this system shows remarkable simplifications. Our estimated critical exponents indicate that $Cr_{1.27}Te_2$ magnetic system can be best described as a quasi-2D Ising system. Therefore, our critical analysis will help to better understand various physical properties reported on this system.

II. Sample Synthesis and Characterizations

Single crystal samples were synthesized by chemical vapor transport (CVT) method. These CVT experiments were performed in a Thermo Scientific Lindberg Blue M three-zone furnace equipped with UP150 model program controllers. Cr (Alfa Aesar, powder, -100+325 mesh, 99.99% metals basis) and Te (Thermo Scientific, shot, 2-5 mm diameter, 99.9999% metals basis) were used as received without further purification. Stoichiometric amounts of Cr and Te are combined in a fused quartz tube. Between 35-50 mg of solid iodine is used as the vapor transport agent. The iodine is added to the tube, which is then sealed under vacuum. The sealed tube is, at minimum, long enough to equal the distance between two zones of a three-zone furnace. This tube is then placed inside the three-zone furnace. All three zones are heated up at a rate of 100°C per hour, with the charge zone reaching 935°C and the crystallization zone reaching 790°C. This temperature gradient is held for one week, then the furnace is cooled at a rate of 100°C per hour to room temperature.

Single crystal X-ray crystallography (hereafter, SCXRD) was used to determine sample phase and composition. All reflection intensities were measured at 293(2) K using a SuperNova diffractometer (equipped with Atlas detector) with Mo $K\alpha$ radiation ($\lambda = 0.71073$ Å) under the program CrysAlisPro (Version CrysAlisPro 1.171.42.49, Rigaku OD, 2022). The same program was used to refine the cell dimensions and for data reduction. The structure was solved with the program SHELXS-2019/3 (Sheldrick, 2018) and was refined on F^2 with SHELXL-2019/3 (Sheldrick, 2018). Analytical numeric absorption correction using a multifaceted crystal model was applied using CrysAlisPro. The temperature of the data collection was controlled using the system Cryojet (manufactured by Oxford Instruments). Table I includes all relevant crystallographic data related to the structure refinement of $Cr_{1.27}Te_2$.

The structure is ordered and is found to be a trigonal system with the space group $P\bar{3}m1$. Initially, the occupancy factors for Te1, Cr1 and Cr2 were set to refine freely, and their values refined to 1 for Te1 and Cr1 while the value for Cr2 was significantly smaller than 1. In the final refinement, the occupancy factors for Te1 and Cr1 were constrained to be 1 while the occupancy factor for Cr2 was set to refine freely, and its final value refines to 0.269(7). Based on this refinement, the chemical formula is $Cr_{1.27}Te_2$. Table I shows results of SCXRD refinements. Here we also include Cr1.27Te2_checkCIF_report.pdf as supplementary material.

The Figure 1(a) shows the refined crystal structure of triagonal $Cr_{1.27}Te_2$ generated by Vesta software packages using the Cr1.27Te2.cif file. Figure 1(b) shows the Laue diffraction pattern

which is used to determine the crystallographic axes of the $Cr_{1.27}Te_2$ crystal used for our magnetic measurements reported here. These crystals have two crystallographically independent Cr sites. While Cr1 sites are fully occupied, Cr2 sites are only partially occupied (Table II). Table III shows all known trigonal Cr-Te binary phases. However, the lattice parameters of our $Cr_{1.27}Te_2$ sample is very close to the lattice parameters of the reported 1*T*-$CrTe_2$ phase[10]. These Cr2 atoms occupy sites between Cr-Te layers of 1*T*-$CrTe_2$ crystal. The unit cell volumes of 1*T*-$CrTe_2$ and $Cr_{1.27}Te_2$ phases are almost the same. However, unit cell length along the *c*-axis has shortened to 6.033 Å in $Cr_{1.27}Te_2$ from 6.20 Å in 1*T*-$CrTe_2$. But the unit cell lengths along the *a, b*-axes are longer in $Cr_{1.27}Te_2$ (3.917 Å) compared to the lengths of those axes in 1*T*-$CrTe_2$ (3.86 Å). Our results are consistent with previously reported $Cr_{1.3}Te_2$ phase[27].

To further verify the elemental stoichiometry of chromium and tellurium, scanning electron microscopy (SEM) and energy dispersive spectroscopy (EDS) studies are performed using a JEOL JSM-IT100 by mounting the single crystal sample on carbon-tape (Figure 1(c)). Figure 1(d) shows EDS spectra from eight points indicated in Figure 1(c). Table IV shows the results of the EDS data, wherein the compositional average of the selected points is 38.07% Cr to 61.93% Te, consistent with the expected $Cr_{1.27}Te_2$ composition estimated from SCXRD study.

Table I. Details of single crystal x-ray crystallography experiment[35].

Crystallographic data	
Chemical formula	$Cr_{1.27}Te_2$
M_r	321.24
Crystal system, space group	Trigonal, $P\bar{3}m1$
Temperature (K)	293(2)
a, *c* (Å)	3.9166 (2), 6.0329 (5)
V (Å^3)	80.15(1)
Z	1
Radiation type	Mo *K*α
μ (mm^{-1})	21.96
Crystal size (mm)	0.05 × 0.03 × 0.01
Data collection details	
Diffractometer	SuperNova, Dual, Cu at zero, Atlas
Absorption correction	Analytical *CrysAlis PRO* 1.171.43.90 (Rigaku Oxford Diffraction, 2023) Analytical numeric absorption correction using a multifaceted crystal model based on expressions derived by R.C. Clark and J.S. Reid.[36] Empirical absorption correction using spherical harmonics, implemented in SCALE3 ABSPACK scaling algorithm.
T_{min}, T_{max}	0.467, 0.790
No. of measured,	2144, 140, 139

independent, and observed [$I > 2\sigma(I)$] reflections	
R_{int}	0.035
$(\sin\theta/\lambda)_{max}$ (Å^{-1})	0.766
Details of Refinement	
$R[F^2 > 2\sigma(F^2)]$, $wR(F^2)$, S	0.016, 0.038, 1.24
No. of reflections	140
No. of parameters	10
$\Delta\rho_{max}$, $\Delta\rho_{min}$ (e Å^{-3})	0.73, -2.39
Software packages	*CrysAlis PRO* 1.171.42.49 (Rigaku OD, 2022), *SHELXS2018*/2 (Sheldrick, 2018), *SHELXL2019*/3 (Sheldrick, 2018), *SHELXTL* v6.10 (Sheldrick, 2008).

Table II: Summary of refinement results.

Atom	Site	*x*	*y*	*z*	Occupancy	Uiso (Å^2)
Te	2d	0.6667	0.3333	0.24905(4)	1.000	0.0111(2)
Cr1	1b	0.0000	0.0000	0.5000	1.000	0.0134(3)
Cr2	1a	1.0000	1.0000	0.0000	0.269(7)	0.0070(11)

Table III: A summary of reported binary Cr-Te phases with *trigonal* symmetry.

Phase	Space group	Crystal System	*a* (Å)	*b* (Å)	*c* (Å)	Volume (Å^3)	Ref.
Cr_2Te_3	$P\bar{3}1c$	Trigonal	6.90	6.90	12.50	514.87	[37]
Cr_5Te_8	$P\bar{3}m1$	Trigonal	7.88	7.88	6.27	336.90	[20]
1*T*-$CrTe_2$	$P\bar{3}m1$	Trigonal	3.86	3.86	6.20	80.13	[10]
$Cr_{1.3}Te_2$	$P\bar{3}m1$	Trigonal	3.91	3.91	5.99		[27]
$Cr_{1.27}Te_2$	$P\bar{3}m1$	Trigonal	3.9166(2)	3.9166(2)	6.0329(5)	80.145(11)	This work

Table IV. Quantitative EDS data for chromium and tellurium composition in $Cr_{1.27}Te_2$ whose data points are shown in the image of Fig.1(c) and spectra in Fig.1(d).

Spot Number	Cr atomic %	Te atomic %
1	37.61	62.39
2	38.14	61.86
3	38.4	61.6
4	38.35	61.64
5	38.28	61.72
6	37.92	62.08
7	37.64	62.36
8	38.2	61.8
Average	38.07	61.93
Deviation	0.3099	0.3112

III. Results and Discussion

A single crystal sample of ~12.9 mg mass was used for all these magnetic studies using a Quantum Design 9 Tesla physical property measurement system (PPMS). Figure 2(a) shows temperature (T) dependent zero-field-cooled (ZFC) and field-cooled (FC) dc magnetization (M) of our sample, measured in a magnetic field, H = 1000 Oe applied in two directions: parallel to the *ab*-plane (red curve) and along the *c*-axis (black curve). For the ZFC studies, the sample was first cooled down to 2 K in zero field, then a 1000 Oe magnetic field was applied, and the dc magnetic moment was measured with increasing temperature. For the FC studies, the dc magnetic moment was measured in the same field afterwards while temperature was reduced. Figure 2(a) clearly shows the presence of a magnetic phase transition around 170 K. A sharp upturn in M(T) was observed for both field directions when temperature was decreased. This is an indication of a paramagnetic (PM) to ferromagnetic (FM) phase transition. The difference of the magnetizations (in the ferromagnetic phase) between two crystallographic directions is very large. The low-temperature FC magnetization along the *c*-axis is almost 13 times larger than that along the *ab*-plane. This indicates the presence of large uniaxial magnetic anisotropy in single crystal $Cr_{1.27}Te_2$ sample. A significant splitting between ZFC and FC curves is seen for low-temperature regions which may be due to magnetic domain creeping effect[38].

Using the data from the Figure 2(a) we calculated dM/dT for both planes and plotted this dM/dT vs. T in Figure 2(b) to determine an approximate Curie temperature (T_C). Figure 2(b) clearly indicates that the transition temperature is near 168 K where minimum values of dM/dT for both directions are located. The dc magnetic susceptibility (χ) with respect to temperature (T) is plotted in Figure 2(c). A fit in the temperature range of 180 - 300 K gives us the Curie-Weiss temperature θ = +173.35±0.096 K for *c*-axis and +169.25±0.115 K for *ab*-plane, signifying the ferromagnetic

nature of this phase transition. The calculated effective moment μ_{eff} = 4.13 ± 0.050 μ_B/Cr along the *c*-axis whereas the effective moment μ_{eff} = 2.98 ±0.016 μ_B/Cr parallel to the *ab*-plane. For a comparison, the theoretical value expected for each Cr^{3+} is 3.87 μ_B and the same for each Cr^{2+} is 2.83 μ_B.

Figure 3(a)-(b) show temperature-dependent magnetic hysteresis along *c*-axis and *ab*-plane, respectively. It is clear from these two figures that ***c***-axis is the magnetic easy axis of this material where magnetization saturates for a lower magnetic field. The saturation field $H_s \approx 0.35$ T at T = 3 K along the *c*-axis. Moreover, the saturation magnetic moments μ_s at T = 3 K for 90 kOe field are 2.22 μ_B/Cr and 2.04 μ_B/Cr for fields parallel to the *c*-axis and *ab*-plane, respectively. Next, we calculate the Rhodes-Wohlfarth ratio (RWR) [39,40] for $Cr_{1.27}Te_2$, which is defined as μ_c /μ_s where μ_c calculated from the effective moment μ_{eff} by the following relation: $\mu_c(\mu_c + 2) = \mu_{eff}^2$ and μ_s is saturation moment in the ordered state. The RWR value is 1 for a localized magnetic system and larger for itinerant magnetic systems. Here we obtain RWR = 1.44 and 1.05 for magnetizations along the *c*-axis and *ab*-plane, respectively, indicating weak itinerant nature of ferromagnetism in $Cr_{1.27}Te_2$.

To explore the nature of the paramagnetic (PM) to ferromagnetic (FM) phase transition in $Cr_{1.27}Te_2$, we further investigate the critical behaviors associated with this magnetic phase transition. The isothermal magnetizations (M vs. H) around Curie temperature (T_C) are measured from T = 146 K up to T = 190 K with 2 K increments. In these isothermal magnetization experiments, magnetic field was ramped up from 0 to 90 kOe keeping the temperature constant. To estimate the critical exponents, we have done this measurement for fields applied parallel to the magnetic easy axis of this material[18,32,41–43]. Figure 4 shows isothermal magnetization M(H) of single crystal $Cr_{1.27}Te_2$ along *c*-axis. The Arrott plot (M^2 vs. H/M)[44] derived from these M(H) curves is shown in Figure 5.

The Arrott-Noakes equation[45] is given by $(H/M)^{1/\gamma} = a\,\varepsilon + b\,M^{1/\beta}$, where $\varepsilon = (T - T_C)/T_C$ is the reduced temperature, *a* and *b* are two constants. For the mean-field model $\beta = 0.5$ and $\gamma = 1$ and these values give us the Arrott plot. If this phase transition can be described well by the mean-field model, then M^2 vs. H/M plot would be a series of parallel straight lines in the high magnetic field range and the isothermal magnetization curve at T_C should pass through the origin. Figure 5 does not satisfy these criteria, indicating that this phase transition cannot be described by the simple mean field model. This is expected because the mean-field model does not consider the effects of spin fluctuation and spin-spin correlation. Therefore, we need to generate a modified Arrott plot to estimate the critical exponents which properly describe this phase transition.

The order of the magnetic phase transition can also be determined from the slope of the curves in the Arrott plot (Figure 5) using the Banerjee's criterion[46]. If the plot has a downward curvature or the slope is positive, then it is a second-order phase transition. On the other hand, if the slope is negative or the plot has upward curvature, then the phase transition is a first-order transition. In our case all curves in the high field region have a downward turn. This signifies a second-order magnetic phase transition in $Cr_{1.27}Te_2$ (Figure 5).

We then have plotted four modified Arrott plots using the β and γ values from four known theoretical models[47]: (1) the 3D-Heisenberg model (β = 0.365, γ = 1.386), (2) the 3D-XY model (β = 0.345, γ = 1.316), (3) the 3D-Ising model (β = 0.325, γ = 1.241), (4) the tri-critical mean-field model (β = 0.25, γ = 1). The results are shown in Figure 6, where isothermal magnetization curves are not parallel in the high field region for all four plots. This implies that the above-mentioned four models do not best describe magnetic phase transition in $Cr_{1.27}Te_2$. To estimate the critical exponents for this material, we need to follow an iterative method which is described next.

The critical behavior of a second-order magnetic phase transition can be characterized in detail by a series of interrelated critical exponents[48]. Near a second-order magnetic phase transition, the correlation length ξ diverges as

$$\xi = \xi_0 |(T - T_C)/T_C|^{-\nu} , \qquad (1)$$

where ν is a critical exponent. This leads to the universal scaling laws for the spontaneous magnetization M_s and the inverse initial magnetic susceptibility χ_0^{-1}. The set of critical exponents β, γ, and δ are determined by the temperature-dependences of spontaneous magnetization $M_S(T)$ below T_C, inverse initial magnetic susceptibility $\chi_0^{-1}(T)$ above T_C, and measured field-dependent isothermal magnetization M(H) at T_C, respectively. The corresponding mathematical expressions are the following:

$$M_s(T) = M_0(T)(-\epsilon)^{\beta}, \epsilon < 0, T < T_C, \quad (2)$$

$$\chi_0^{-1}(T) = (h_0/m_0)(\epsilon)^{\gamma}, \epsilon > 0, T > T_C, \quad (3)$$

$$M = DH^{1/\delta}, \ \epsilon = 0, T = T_C. \qquad (4)$$

Here $\varepsilon = (T-T_C)/T_C$, and M_0, h_0/m_0, and D are called critical amplitudes[49].

To estimate the appropriate critical exponents and Curie temperature for $Cr_{1.27}Te_2$ magnetic phase transition, a rigorous iterative method was used, which was initially proposed by Pramanik and Banerjee[50]. A linear extrapolation of each isothermal magnetization curve of the (modified) Arrott plot from the high magnetic field regime to the $M^{1/\beta}$ and $(H/M)^{1/\gamma}$ axis will yield $M_s(T)$ and $1/\chi_0(T)$ values, respectively. Next, we use these estimated $M_S(T)$ and $1/\chi_0(T)$ values to get a new set of β and γ by fitting them to Equations (2) and (3).

This new set of β and γ is then used to reconstruct a new modified Arrott plot. This above-mentioned procedure is then repeated until the values of β, γ, and T_C reach respective stable values. It is worth noting that the exponents generated by this method are independent of the initial parameters, which signifies the reliability of these estimated critical exponents. Following this procedure, we estimate critical exponents β = 0.2653±0.007 with T_C = 168.73±0.066 K and γ = 1.2298±0.004 with T_C = 169.01±0.034 K using equations 2 and 3.

Figure 7 shows the final modified Arrott plot, plotted using the above-mentioned critical exponent values and Curie temperature. A set of parallel straight lines at high magnetic fields in Figure 7 shows proper estimation of β and γ values as described above. Figure 8 shows the final M_S (T) and

$1/\chi_0(T)$ with the best-fitted curves (solid red lines) to Equations 2 and 3. Next, we use the Kouvel-Fisher (KF) method for a better estimation of these two critical exponents[51].

According to Kouvel and Fisher, following relations hold for a 2nd order magnetic phase transition:

$$\frac{M_S(T)}{\frac{dM_S(T)}{dT}} = \frac{T-T_C}{\beta} \qquad (5)$$

$$\frac{\frac{1}{\chi_0(T)}}{\frac{\mathrm{d}(\frac{1}{\chi_0})(T)}{\mathrm{d}T}} = \frac{T-T_C}{\gamma} \qquad (6)$$

Figure 9 shows the Kouvel-Fisher plot, plotted using the M_S (T) and $1/\chi_0(T)$ obtained from the final Arrott plot. By fitting the data to the Equations 5 and 6, in the regime below and above T_C we estimate β = 0.2631(±0.002) with T_C = 168.91(±0.061) K, and γ = 1.2314(±0.007) with T_C = 168.48(±0.31) K, respectively. The values of β, γ, and T_C estimated from the KF method are consistent with those obtained from the iterative modified Arrott plot (MAP), implying that the critical values are reliable and intrinsic.

The critical exponent δ can be obtained by analyzing the critical isothermal magnetization M(H) at T_C (Equation 4). We already determined $T_C \approx 168.5$ K from our critical analysis. We then estimate δ = 5.31(±0.024) by fitting Equation 4 to the isothermal magnetization at T_C at higher field region (for H > 1 kOe) (Figure 10). According to the statistical theory, these three critical exponents satisfy a Widom scaling relation[52]:

$$\delta = 1 + \frac{\gamma}{\beta}. \qquad (7)$$

Using the Widom scaling relation, we estimate critical exponent δ = 5.52 and 5.61 by using the β and γ values estimated by MAP and KF methods, respectively, which is in good agreement with the δ = 5.31(±0.024) value we estimate from the critical isotherm analysis.

The critical exponents obtained from MAP, KF method, and the critical isotherm method are listed in Table V. The critical exponents β and δ values are very close to the tri-critical mean-field values. But the γ value lies in between 3D Ising and tri-critical mean-field model values, but closer to the 3D Ising model value. This implies that interlayer couplings play important roles in this material. Taroni *et al.* have shown that the critical exponent β of 2D magnets is within the range of $0.1 \leq \beta \leq 0.25$. Our estimated β value is very close to this range, hence there is a possibility that this material may behave as a 2D Ising magnet[53].

The accuracy of our estimated critical exponents can be further verified following the prediction of the scaling hypothesis. In the critical region, the magnetic equation can be written as:

$$M(H, \varepsilon) = \varepsilon^{\beta} f_{\pm}(H/\varepsilon^{\beta+\gamma}), \qquad (8)$$

where the functions f_+ and f_- are functions valid in the T > Tc and T < Tc regimes, respectively. Moreover, the Equation 8 can also be re-written as:

$$m = f_{\pm}(h), \qquad (9)$$

where the renormalized magnetization $m \equiv \varepsilon^{-\beta} M(H,\varepsilon)$ and the renormalized magnetic field $h \equiv \varepsilon^{-(\beta+\gamma)} H$. This scaling hypothesis in Eq. (9) implies that, with reasonably accurate values of β and γ, the $M\,|\varepsilon|^{-\beta}$ vs. $H\,|\varepsilon|^{-(\beta+\gamma)}$ plots in the critical region should collapse onto two universal curves: one for the temperatures above T_C and the other for the temperatures below T_C[48]. The normalized m ($\equiv M|\varepsilon|^{-\beta}$) vs. normalized h ($\equiv H|\varepsilon|^{-(\beta+\gamma)}$) are plotted in Fig.11(a). Clearly, the lines form two different groups: one above and another below T_C. This is an important check of accuracy of our critical analysis. This can be further verified by a more rigorous method using m^2 vs. h/m plot, also known as the normalized Arrott plot, as shown in Fig. 11(b), in which all these curves collapse into two different branches. This is also another verification of the accuracy of the estimated critical exponents. Furthermore, the scaling equation of state can be written in another form:

$$\frac{H}{M^{\delta}} = k\left(\frac{\varepsilon}{H^{1/\beta}}\right), \qquad (10)$$

where $k(x)$ is a scaling function. According to Eq. (10), all experimental curves will collapse into a single curve. Figure 12 shows $MH^{-1/\delta}$ vs. $\varepsilon H^{-1/(\beta\delta)}$ plot for $Cr_{1.27}Te_2$, where all isothermal magnetizations collapse into a single curve, and T_C is located at the zero point in the horizontal axis. This properly scaled curves further verify the reliability of our estimated critical exponents.

Next, it is important to understand the nature and range of magnetic interactions in this material. In a homogeneous magnet the universality class of the magnetic phase transition depends on the exchange distance J(*r*). Fisher *et al*. theoretically treated this kind of long-range magnetic ordering as an attractive interaction between spins[54]. In the renormalization group theory analysis, the long-range interaction decays with distance *r* as

$$J(r) \approx r^{-(d+\sigma)} \quad (11),$$

where σ is a positive constant and *d* is the crystal dimensionality. Moreover, the magnetic susceptibility critical exponent γ can be expressed as

$$\gamma = 1 + \frac{4}{d}\left(\frac{n+2}{n+8}\right)\Delta\sigma + \frac{8(n+2)(n-4)}{d^2(n+8)^2} \times \left[1 + \frac{2G\left(d/2\right)(7n+20)}{(n-4)(n+8)}\right]\Delta\sigma^2 \quad (12)$$

Where $\Delta\sigma = \left(\sigma - \frac{d}{2}\right)$ and $G\left(\frac{d}{2}\right) = 3 - \frac{1}{4}\left(\frac{d}{2}\right)^2$, and *n* is spin dimensionality[55]. The renormalization group theory analysis also implies that the characteristic length scale of spin interaction is short- or long-range depending on σ > 2 or σ < 2, respectively. However, σ value also depends on *d* and *n* values. Since, these values are not known a priori, we use the following analysis to determine the most appropriate σ value for this system. First, we calculate σ from Equation 12 using the estimated γ = 1.231 (from the KF method) and a chosen set of *d* and *n* values. Using this calculated σ value, we then calculate other critical exponents sequentially from the following expressions: ν = γ/σ, α = 2 − ν*d*, β = (2 − α − γ)/2, δ = 1 + γ/β. Table VI shows calculated σ, β, γ, and δ values for

various combinations of *d* and *n* values. If the calculated values of critical exponents (shown in Table VI) are in good agreement with our estimated critical exponent values (shown in Table V), then that is the appropriate choice of *d* and *n* values for this system and the corresponding σ value will determine the spin-spin interaction range here.

It is clear from this Table VI that our calculated critical exponents for these *d* and *n* values do not match well with our estimated critical exponent values (in Table V). However, for {d: n} = {2:1}, the calculated critical exponents (β = 0.3115, γ = 1.4225, and δ = 5.5666) have closest match with the estimated critical exponent values from KF method (β = 0.2631, γ = 1.2314, and δ = 5.61). These β and γ values are also closer to the critical exponent values for 2D long-range interaction (β = 0.298, γ = 1.398, and δ = 5.67) model[55]. As previously discussed, Taroni *et al.* has reported that the β value of any 2D system should be in the window $0.1 < \beta < 0.25$[53]. Our estimated β value for $Cr_{1.27}Te_2$ is 0.263 (from the Kouvel-Fisher method). But our renormalization group theory analysis suggests that spin interaction in $Cr_{1.27}Te_2$ could be best described as the 2D Ising ({d: n} = {2:1}) type. The Ising nature of this spin system is further corroborated by the highly anisotropic in- and out-of-plane magnetic responses as shown in Figures 2(a) and 3. Hence, we conclude that single crystal $Cr_{1.27}Te_2$ is a quasi-2D Ising system coupled with a long-range (σ = 1.26) interaction between these spins. This long-range interaction will decay as $J(r) \approx r^{-3.26}$.

IV. Conclusion

In summary, high-quality single-crystal $Cr_{1.27}Te_2$ samples have been grown by the chemical vapor transport method and confirmed by single-crystal X-ray diffraction studies. We perform a comprehensive study of its critical behavior around the PM-FM transition in bulk $Cr_{1.27}Te_2$ crystal. The PM-FM phase transition in $Cr_{1.27}Te_2$ is second order in nature. The critical exponents β, γ, and δ estimated from various methods (MAP, KF plot, critical isotherms) match well and follow the universal scaling analysis, suggesting the accuracy of our estimation. The estimated critical exponents match well with those calculated from the results of the renormalization group approach for a quasi-2D Ising ({d: n} = {2:1}) system coupled with a long-range interaction between spins.

Supplementary materials

As mentioned earlier, here we also include Cr1.27Te2_checkCIF_report.pdf as supplementary material. The Crystallographic Information File (cif) file of $Cr_{1.27}Te_2$ is analyzed and described in the supplementary material which properly justifies our structural characterization.

Acknowledgements

This work is supported by the National Science Foundation Awards No. DMR-2018579 and No. DMR-2302436. This work made use of the synthesis facility of the Platform for the Accelerated Realization, Analysis, and Discovery of Interface Materials (PARADIM), which is supported by the National Science Foundation under Cooperative Agreement No. DMR-2039380. We are thankful to Dr. Maxime Siegler of Johns Hopkins University for SCXRD experiments.

*Address of correspondence: samaresh.guchhait@howard.edu.

Table V: A comparison of our estimated critical exponents of $Cr_{1.27}Te_2$ with critical exponents of other Cr-Te binary phases and different theoretical models.

Composition	Technique	β	γ	δ
$Cr_{1.27}Te_2$ (this work)	Modified Arrott Plot	0.265±0.007	1.229±0.004	5.52*
$Cr_{1.27}Te_2$ (this work)	Kouvel-Fisher Method	0.263±0.002	1.231±0.007	5.61*
$Cr_{1.27}Te_2$ (this work)	Isothermal Magnetization at T_C = 168.5 K			5.310±0.024
Theory[44]	Mean Field Model	0.5	1	3
Theory[47]	3D Ising Model	0.325	1.24	4.80
Theory[47]	3D Heisenberg Model	0.365	1.386	4.82
Theory[47]	3D XY Model	0.345	1.361	4.81
Theory[47]	Tri-critical Mean Field Model	0.25	1	5
Cr_4Te_5[32]	Kouvel-Fisher Method	0.387	1.287	4.32

Cr_5Te_8[18]	Kouvel-Fisher Method	0.321	1.27	4.9
$Cr_{0.62}Te$[6]	Kouvel-Fisher Method	0.315	1.81	6.75
Cr_5Te_8[19]	Magnetocaloric effect	0.362	1.399	4.86
Cr_5Te_6[34]	Kouvel-Fisher Method	0.406	1.199	3.95
Cr_3Te_4 [33]	Kouvel-Fisher Method	0.3817	1.2119	4.16

*Estimated by Widom scaling relation.

Table VI: Critical exponents calculated from the renormalization group theory analysis for various combinations of *d* and *n* values (see text for details).

d	*n*	σ	β	γ	δ
3	1	1.89	0.36	1.2314	4.42
3	2	1:85	0.3875	1.2314	4.1778
3	3	1.83	0.3912	1.2314	4.1477
2	1	1.26	0.3115	1.4225	5.5666
2	2	1.21	0.3456	1.0663	4.0846
2	3	1.67	0.1215	1.4768	13.1025

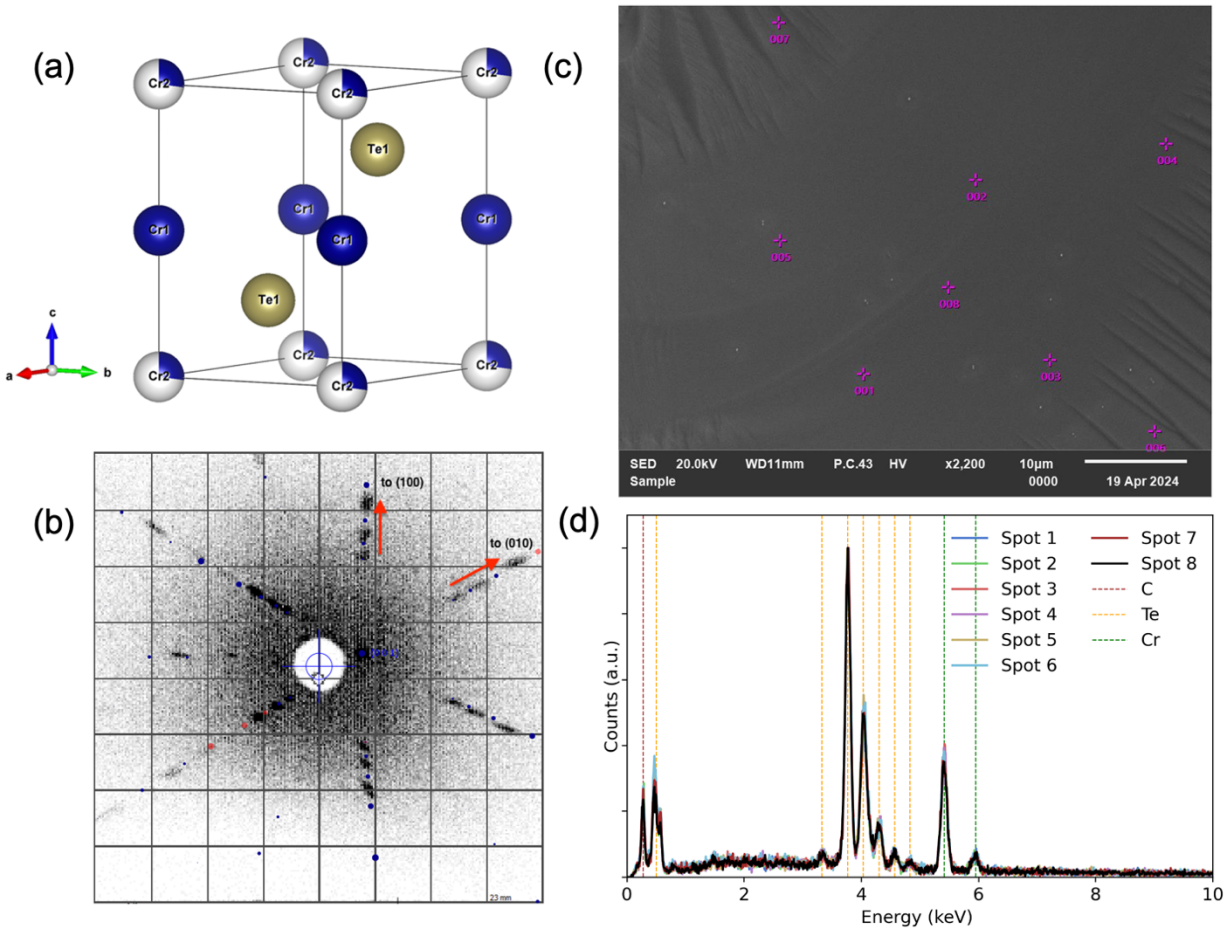

Figure 1: (a) View of the refined crystallographic unit cell generated by VESTA software package. (b) Laue diffraction image of the single crystal $Cr_{1.27}Te_2$ sample. The sample is oriented along the crystallographic (001) axis. Arrows show the direction to the other crystallographic axes, as simulated by the QLaue software. (c) SEM image of $Cr_{1.27}Te_2$ crystal with eight purple points denoting EDS locations. (d) EDS spectra of the $Cr_{1.27}Te_2$ crystal from the eight points shown in Fig. 1(c). The carbon peaks are most likely due to carbon-tape sample holder.

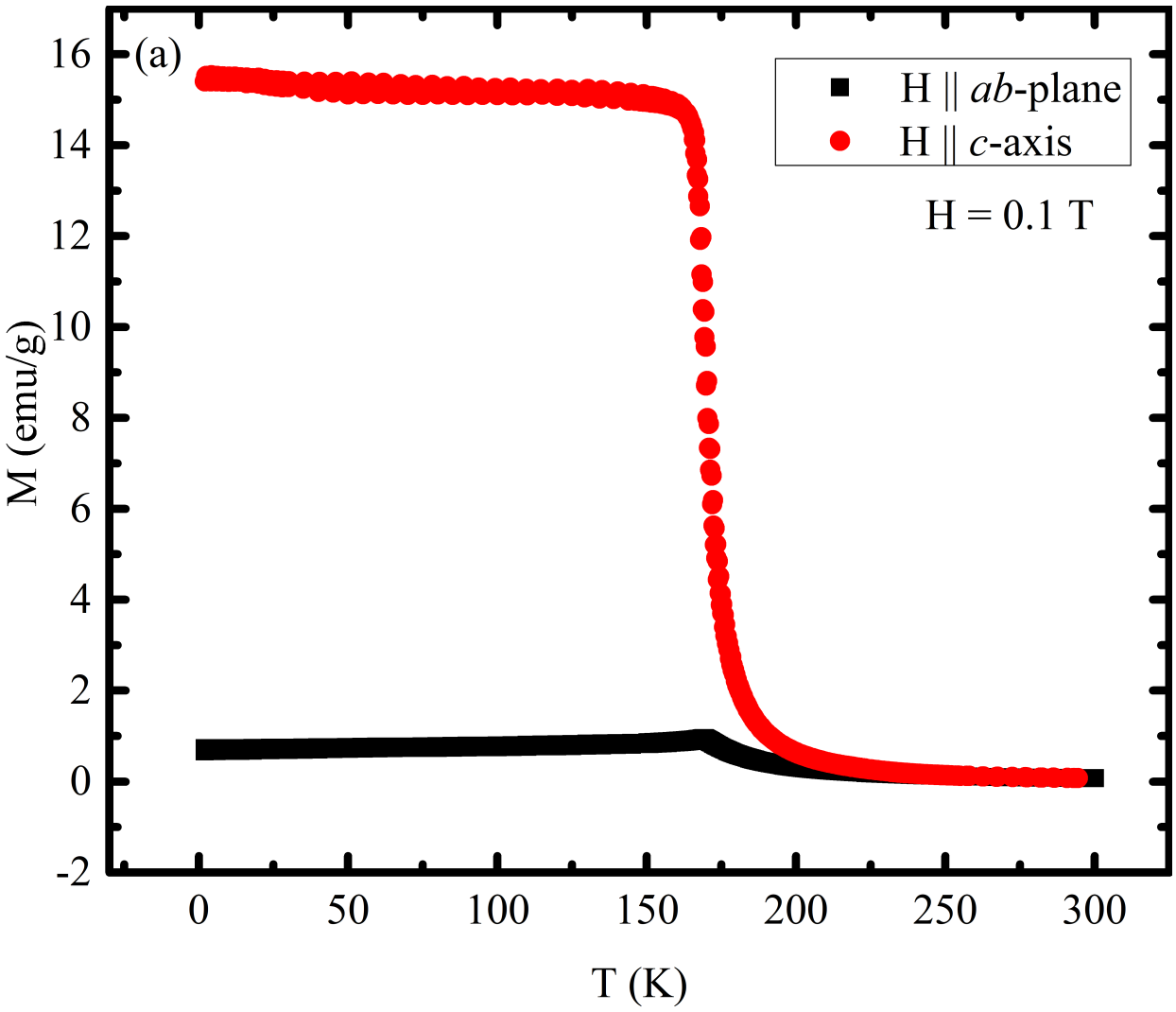
(a)
H || ab-plane
H || c-axis
H = 0.1 T
M (emu/g)
T (K)
16
14
12
10
8
6
4
2
0
-2
0
50
100
150
200
250
300

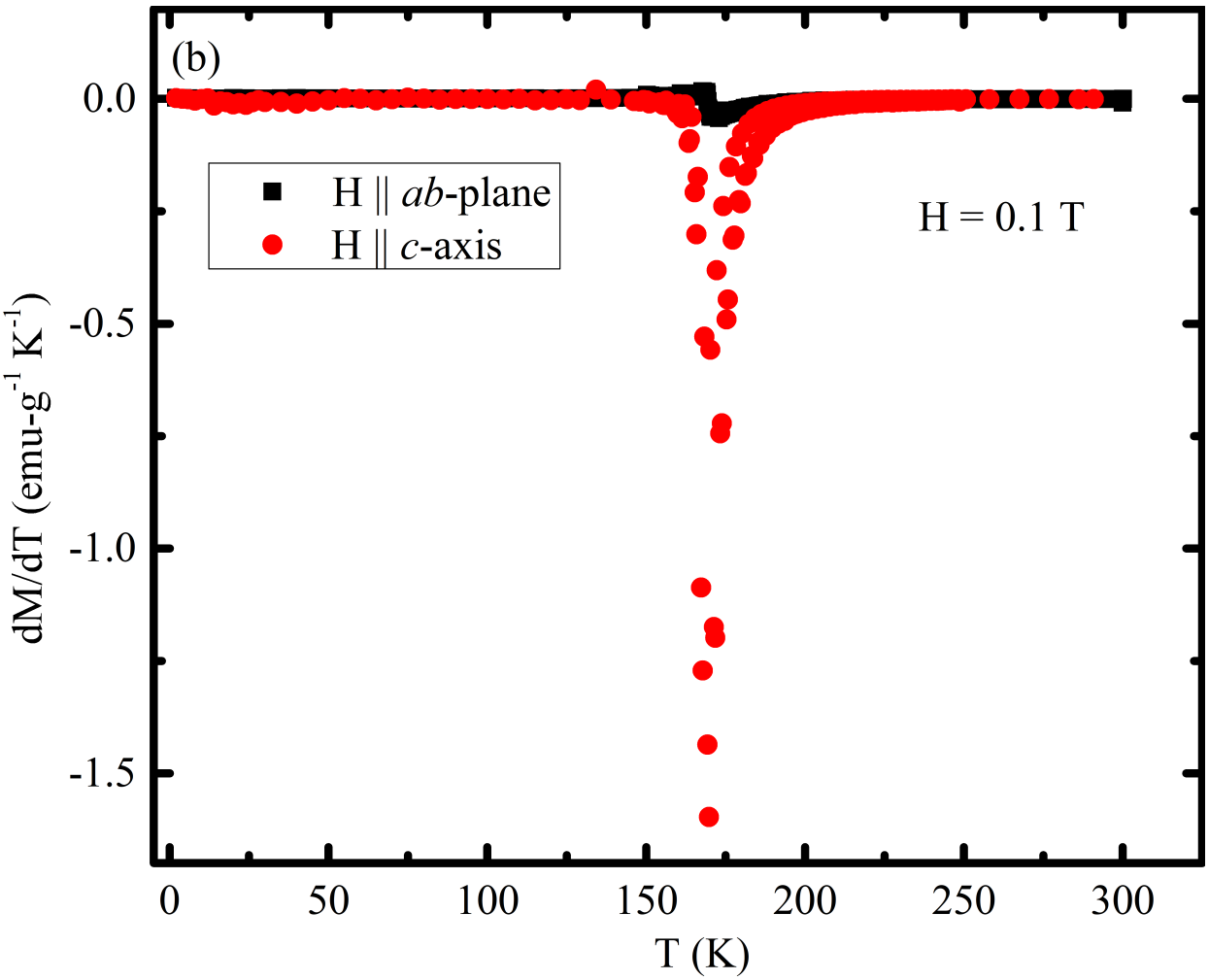
(b)
H || ab-plane
H || c-axis
H = 0.1 T
dM/dT (emu-g-1 K-1)
0.0
-0.5
-1.0
-1.5
0
50
100
150
200
250
300
T (K)

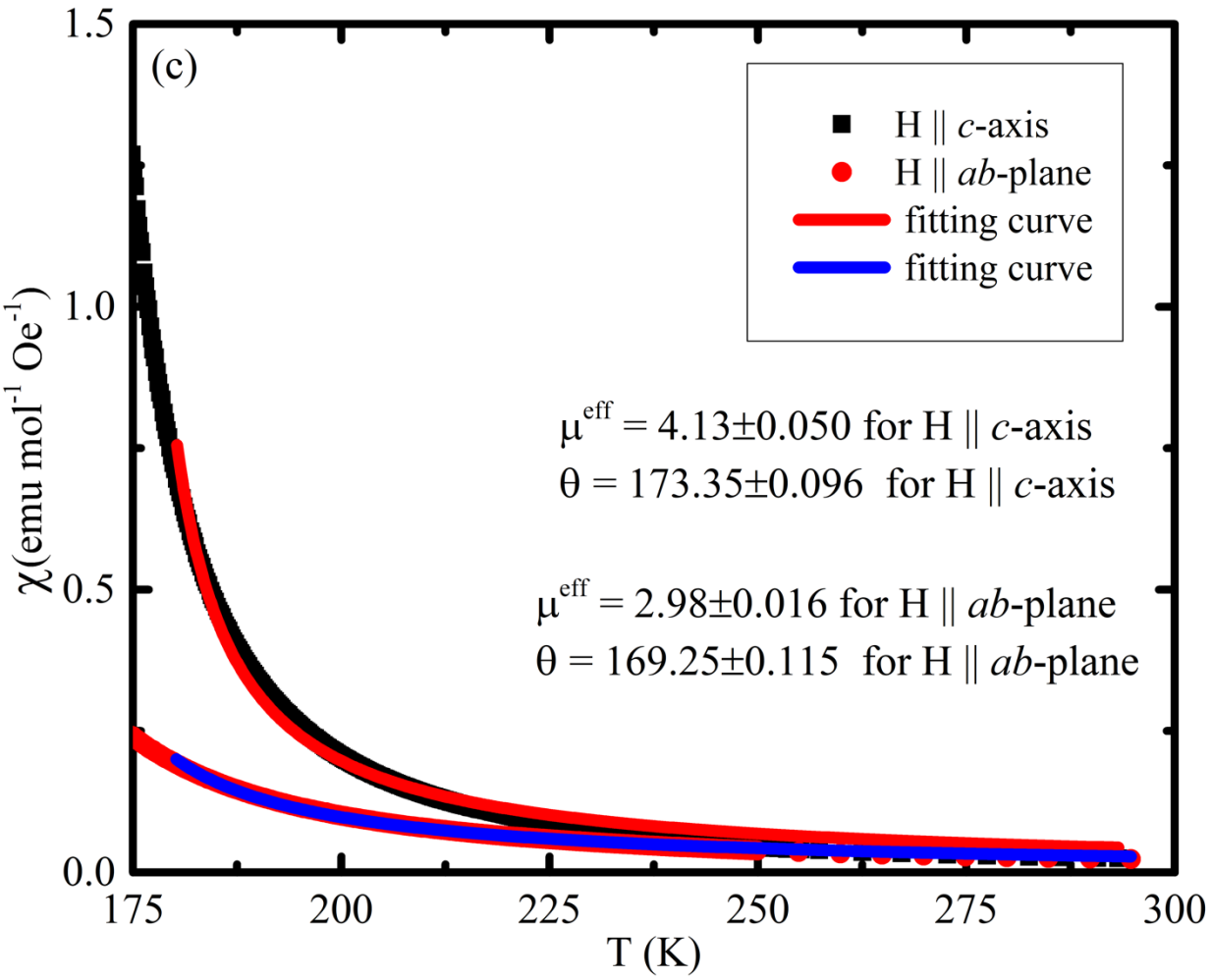

Figure 2: (a) Temperature (T) dependent dc magnetization (M) measured with the application of 1000 Oe magnetic field parallel to the *ab*-plane (red curve) and along the *c*-axis (black curve) with both zero-field cooled (ZFC) and field cooled (FC) mode. (b) This figure shows the temperature dependence of dM/dT near the magnetic phase transition temperature for both magnetizations along the *ab*-plane and *c*-axis. (c) The temperature dependent magnetic susceptibility of $Cr_{1.27}Te_2$ for magnetic field applied parallel to the *ab*-plane (black data and red fitted curve) and along the *c*-axis (red data and blue fitted curve). We obtained the best fitted curves by fitting our data to the Curie-Weiss law $\chi = C/(T-\theta)$.

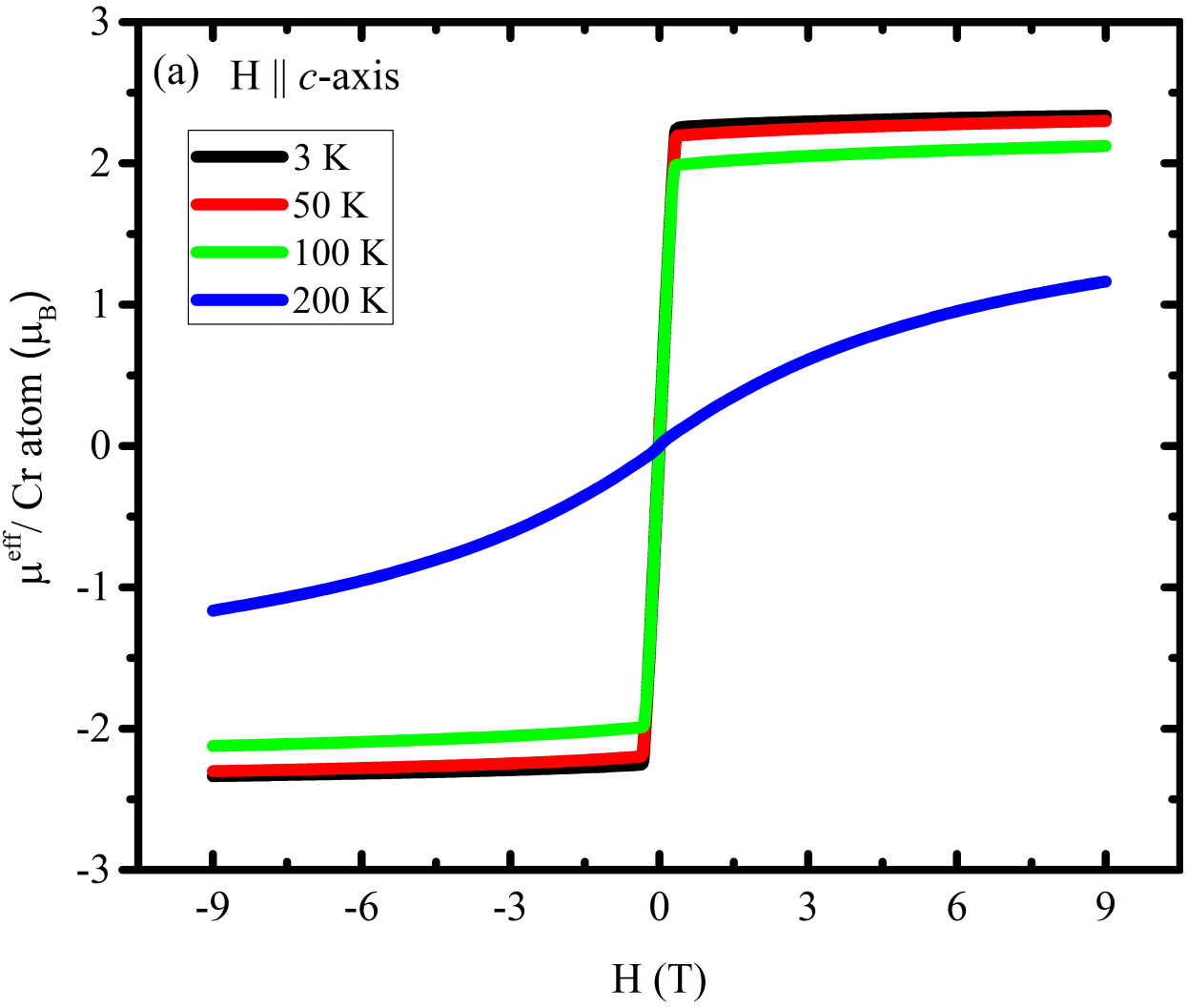
(a) H || c-axis
3 K
50 K
100 K
200 K
μ^eff / Cr atom (μ_B)
H (T)
3
2
1
0
-1
-2
-3
-9
-6
-3
0
3
6
9

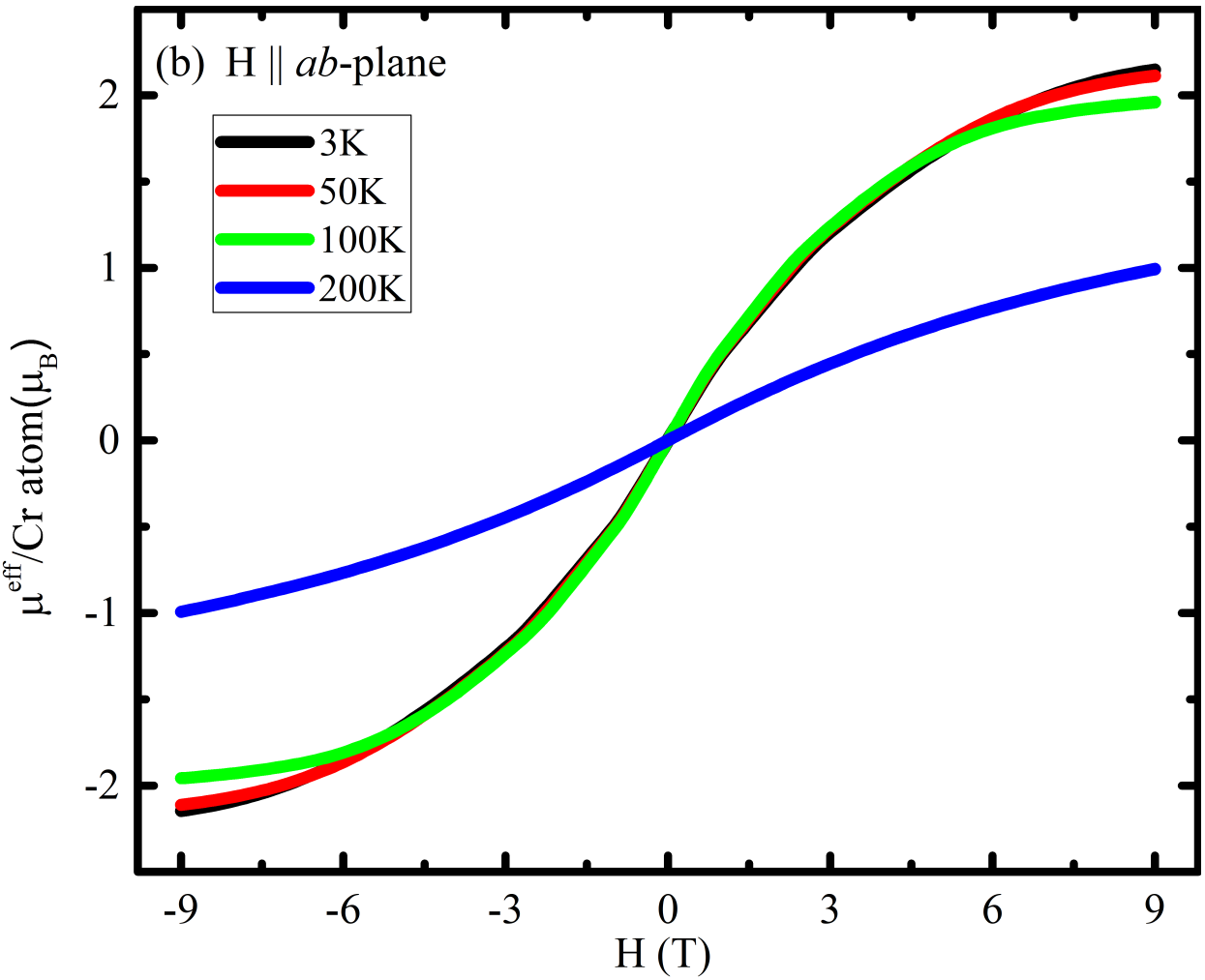

Figure 3: (a) Temperatures-dependent magnetic hysteresis of a single crystal $Cr_{1.27}Te_2$ sample performed along the *c*-axis. (b) Temperatures-dependent magnetic hysteresis of a single crystal $Cr_{1.27}Te_2$ sample performed parallel to the *ab*-plane.

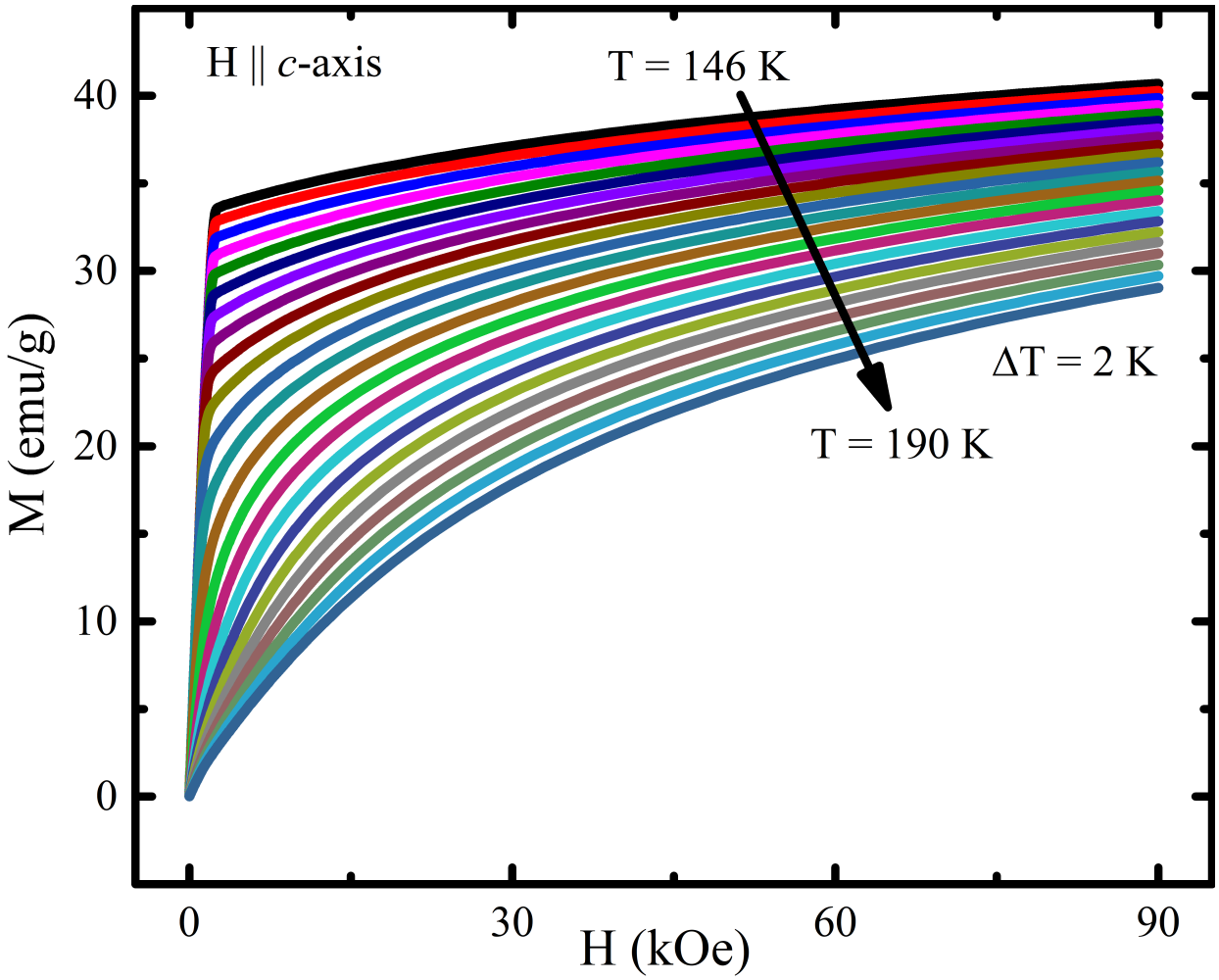

Figure 4: The isothermal magnetization measured along the *c*-axis at 2 K interval around the magnetic phase transition temperature of single-crystal $Cr_{1.27}Te_2$.

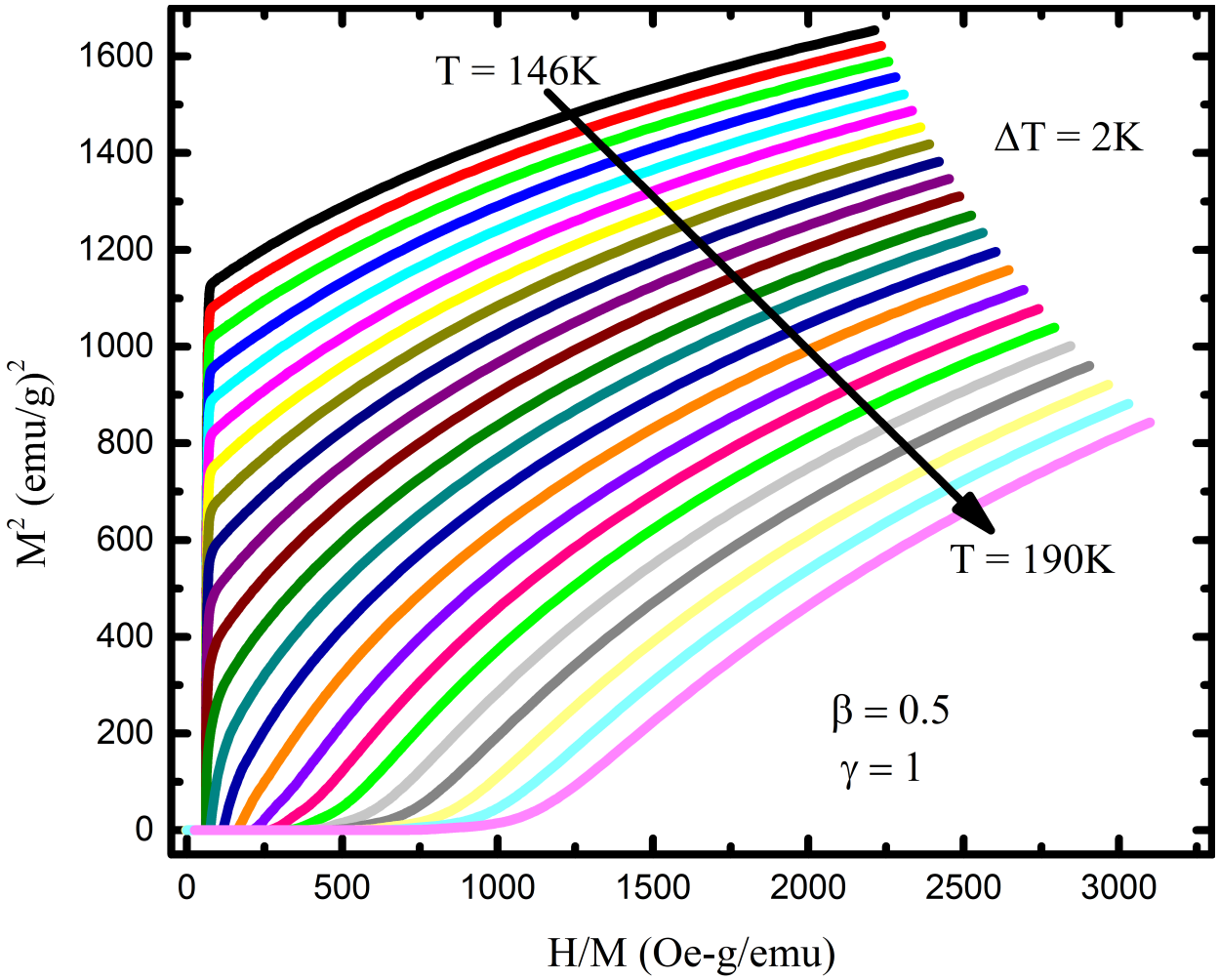

Figure 5: The Arrott plot of isothermal magnetizations along the *c*-axis of a single crystal sample shows clear deviation from the mean-field model description of $Cr_{1.27}Te_2$ magnetic phase transition.

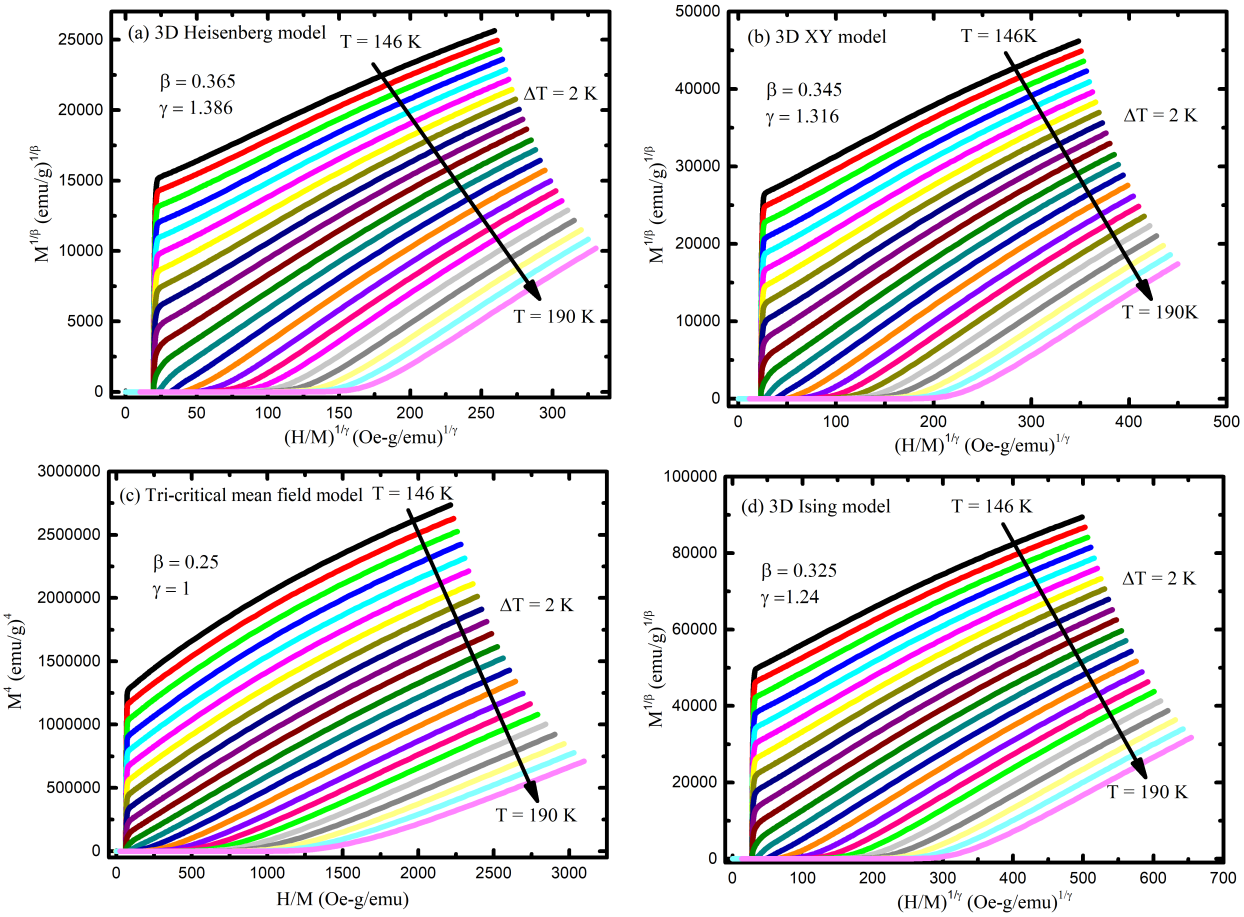

Figure 6: Modified Arrott plots of isothermal magnetizations plotted using known β and γ values from four models: (a) 3D Heisenberg model, (b) 3D XY model, (c) tri-critical mean field model, and (d) 3D Ising model.

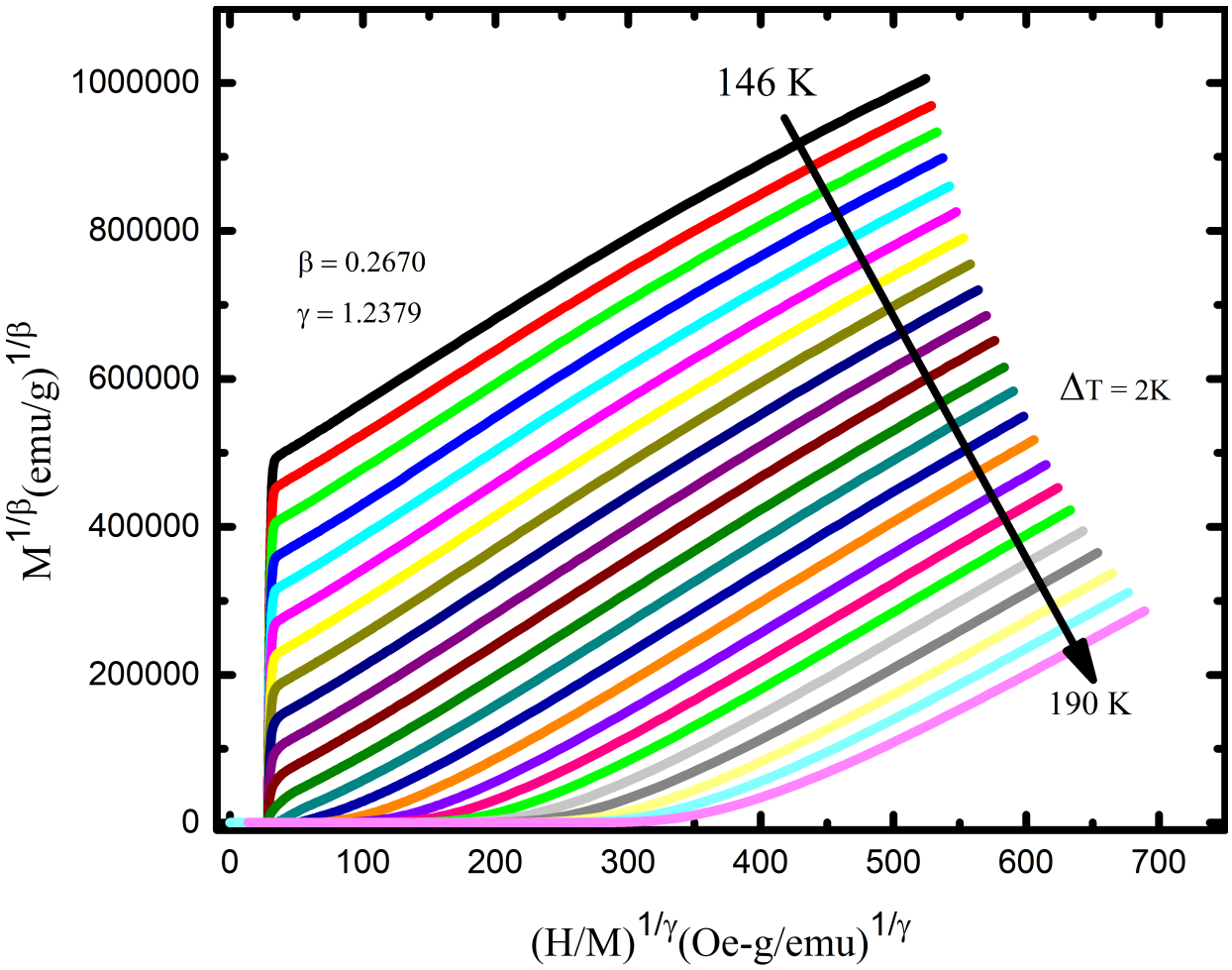

Figure 7: The modified Arrott plot of the isothermal magnetizations around the magnetic phase transition temperature plotted with the best estimated critical exponent values of β = 0.2613 and γ = 1.2342.

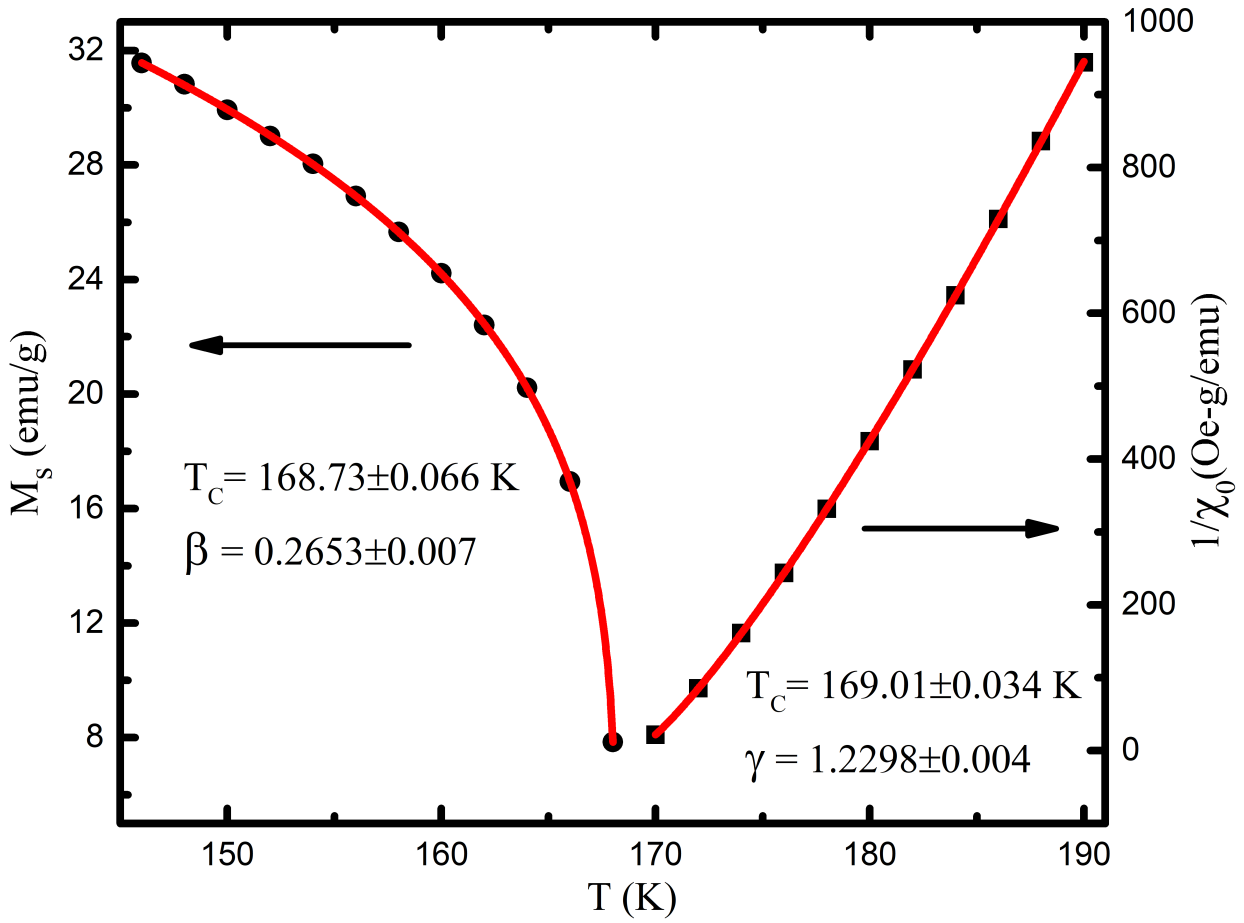

Figure 8: Temperature dependent spontaneous magnetization (M_S) and inverse initial susceptibility (χ_0^{-1}) are plotted around the magnetic phase transition. M_S and χ_0^{-1} are extracted by extrapolating the modified Arrott plot at high field regions. Estimated β = 0.2653(±0.007) & T_C =168.73±0.066 K, and γ = 1.2298±0.004 & T_C = 169.01±0.034 K values are shown in this figure.

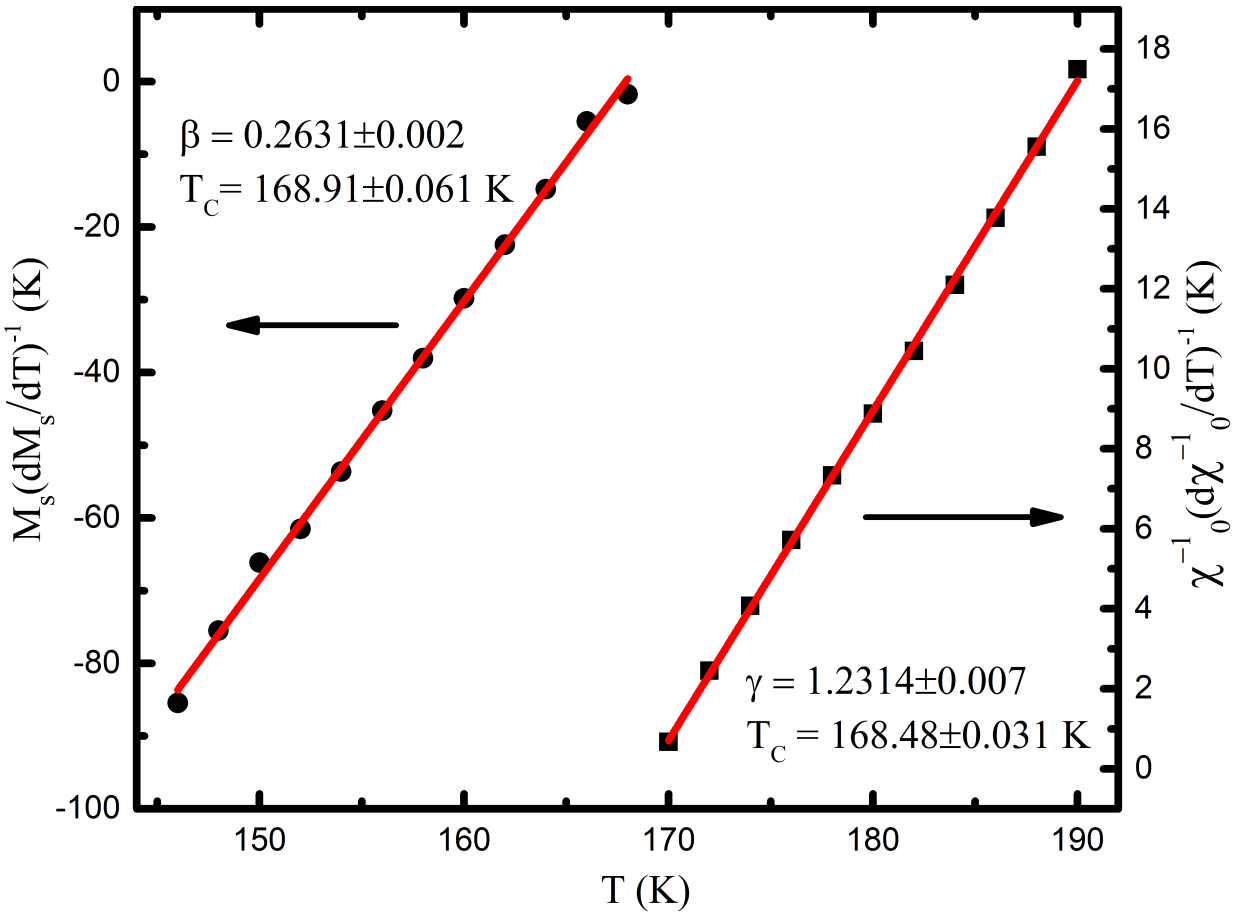

Figure 9: The Kouvel-Fisher plot shows the temperature dependencies of $M_s(T)/[dM_s(T)/dT]^{-1}$ (star symbol) and $\chi_0^{-1}(T)/[d\chi_0^{-1}(T)/dT]$ (squares) for single crystal $Cr_{1.27}Te_2$ sample. The best estimated $\beta = 0.2631 \pm 0.002$ & $T_C = 168.91 \pm 0.061$ K, and $\gamma = 1.2314 \pm 0.007$ & $T_C = 168.48 \pm 0.031$ K values are indicated in this figure.

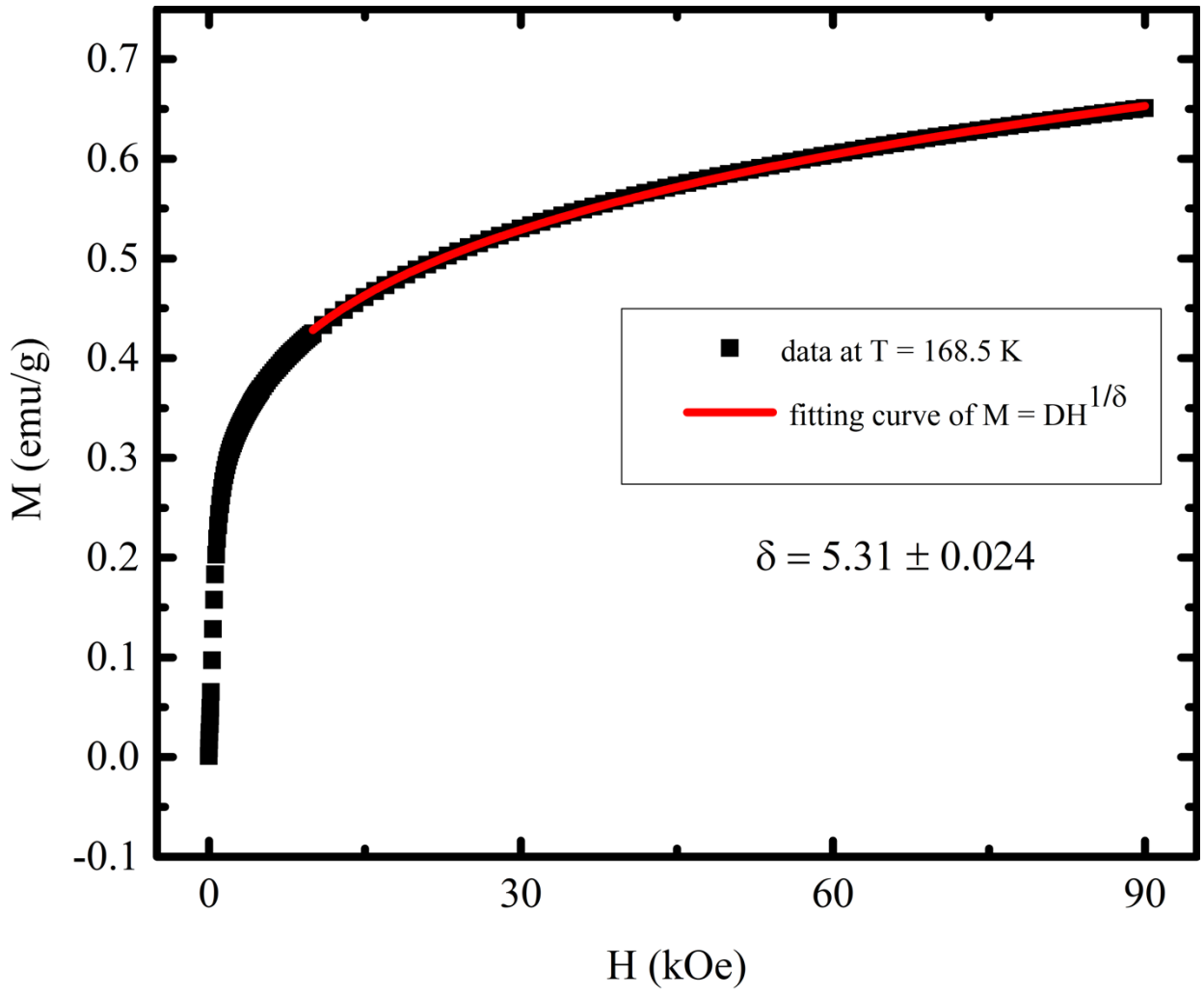

Figure 10: The isothermal magnetization at T_C = 168.5 K along the *c*-axis of single crystal $Cr_{1.27}Te_2$ sample gives an estimated δ = 5.31(±0.004).

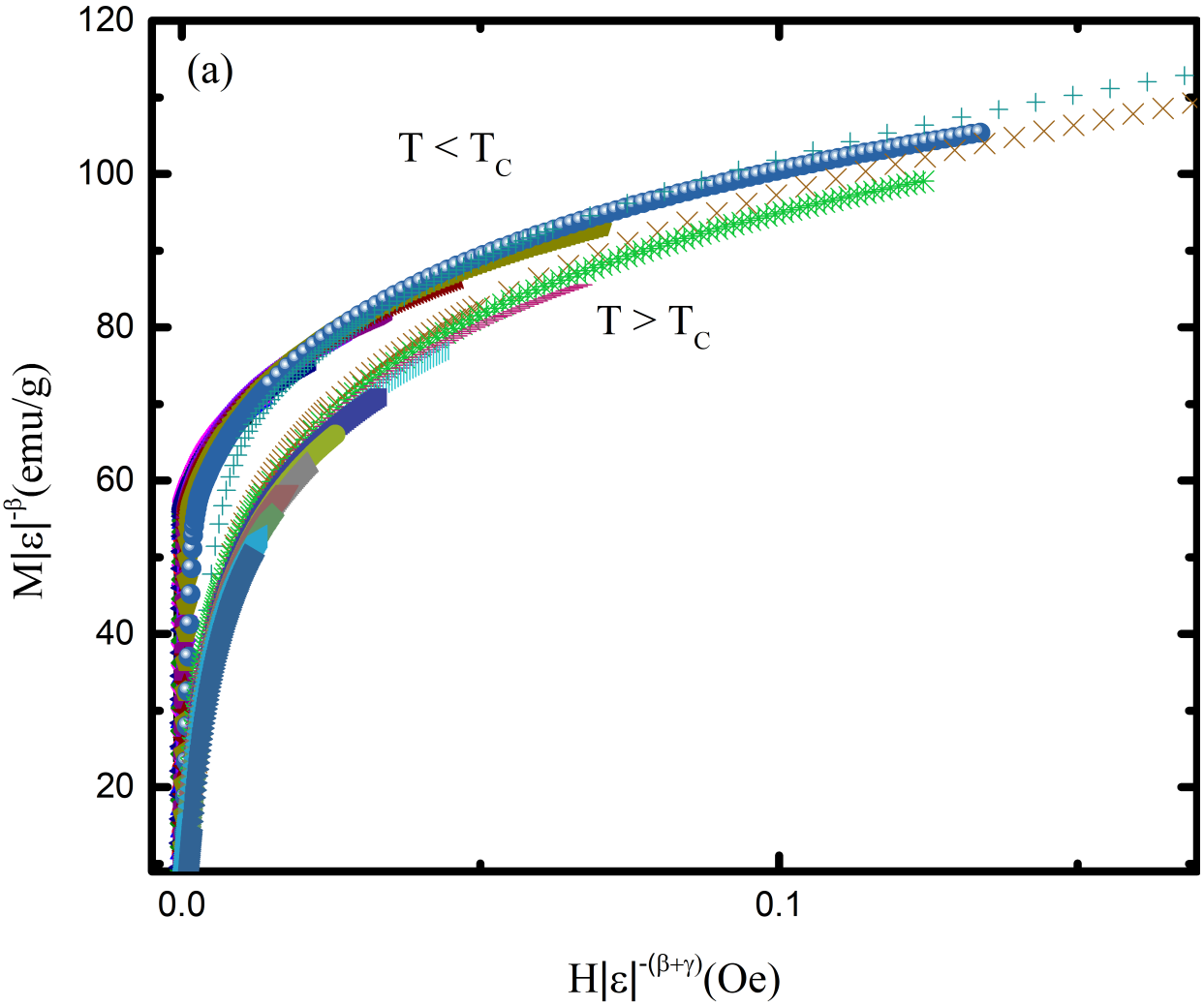
(a)
T < T_C
T > T_C
120
100
80
60
40
20
0.0
0.1
M|ε|^-β(emu/g)
H|ε|^-(β+γ)(Oe)

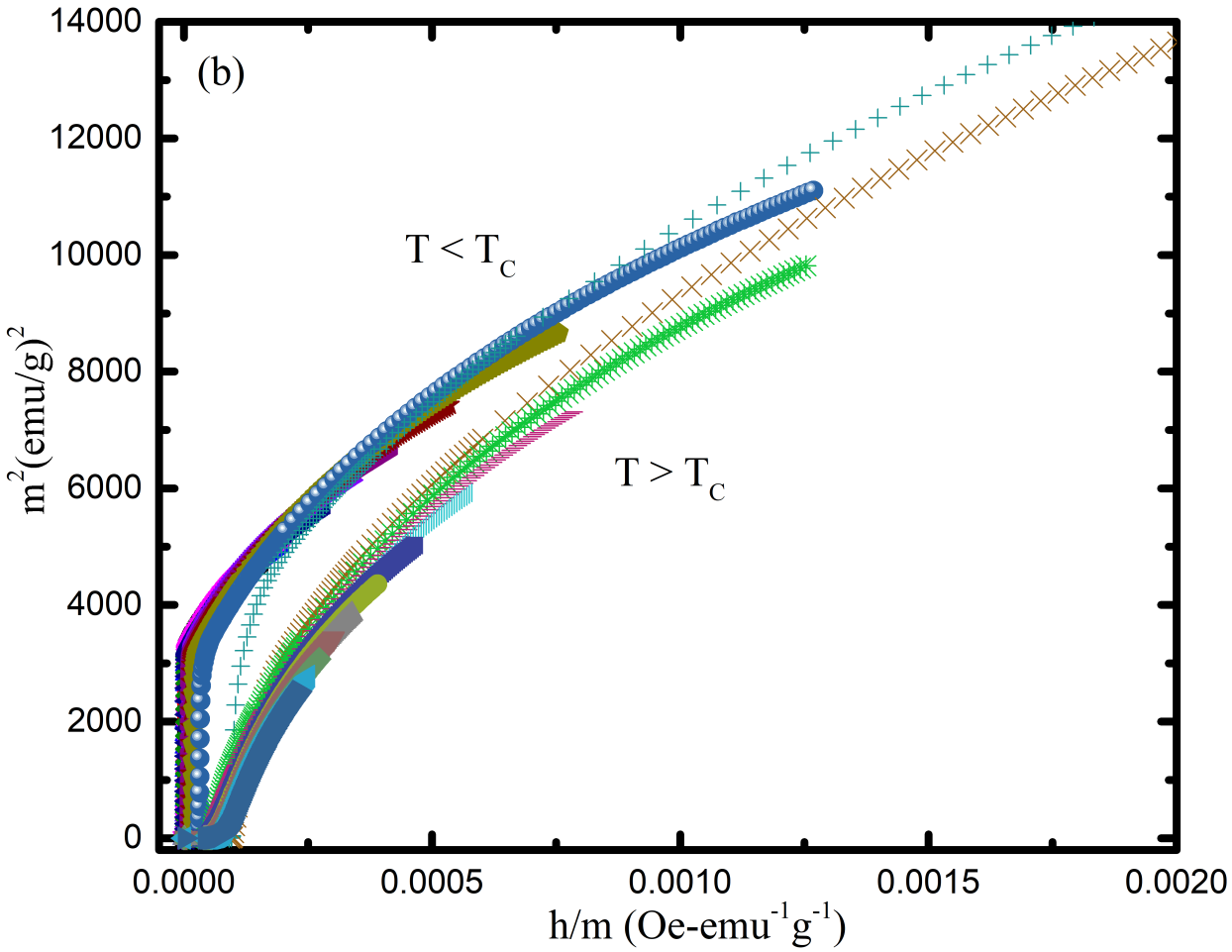

Figure 11: Verification of reliability of our critical analysis: (a) A plot of normalized magnetization ($m = M|\varepsilon|^{-\beta}$) as a function of normalized field ($h = H|\varepsilon|^{-(\beta+\gamma)}$) of isothermal magnetizations scale into two groups: one below T_C and another above the T_C. This plot shows the accuracy of our critical exponent analysis. (b) The normalized magnetization (m^2) as a function of normalized inverse magnetic susceptibility (h/m) for different temperatures also scales into two groups validating accuracy of our critical analysis.

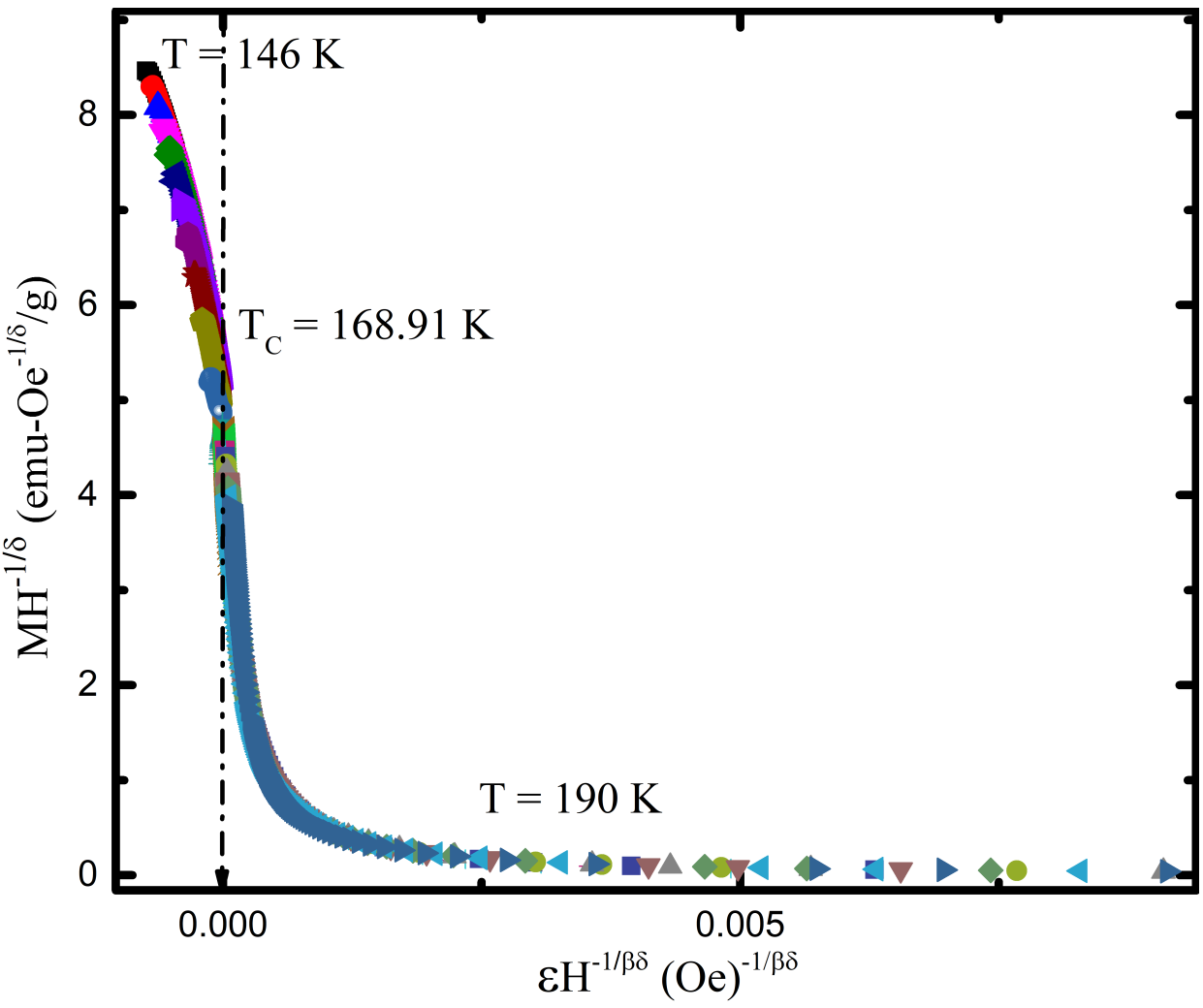

Fig.12. All temperature-dependent isothermal magnetization M(H) data maps onto one curve when they are plotted as $MH^{-1/\delta}$ vs. $\varepsilon H^{-1/\beta\gamma}$.

References:

[1] C. Gong, L. Li, Z. Li, H. Ji, A. Stern, Y. Xia, T. Cao, W. Bao, C. Wang, Y. Wang, Z.Q. Qiu, R.J. Cava, S.G. Louie, J. Xia, and X. Zhang, "Discovery of intrinsic ferromagnetism in two-dimensional van der Waals crystals," Nature **546**(7657), 265–269 (2017).

[2] Y. Zhu, X. Kong, T.D. Rhone, and H. Guo, "Systematic search for two-dimensional ferromagnetic materials," Phys Rev Mater **2**(8), 81001 (2018).

[3] H. Sato, M. Koyama, K. Takada, H. Okuda, K. Shimada, Y. Ueda, J. Ghijsen, and M. Taniguchi, "Electronic structure of chromium chalcogenides," J Electron Spectros Relat Phenomena **88–91**, 333–337 (1998).

[4] H. Ipser, K.L. Komarek, and K.O. Klepp, "Transition metal-chalcogen systems viii: The Cr□Te phase diagram," Journal of the Less Common Metals **92**(2), 265–282 (1983).

[5] G. Chattopadhyay, "The Cr-Te (Chromium-Tellurium) System," Journal of Phase Equilibria **15**(4), 431–440 (1994).

[6] Y. Liu, and C. Petrovic, "Critical behavior of the quasi-two-dimensional weak itinerant ferromagnet trigonal chromium telluride ${\mathrm{Cr}}_{0.62}\mathrm{Te}$," Phys Rev B **96**(13), 134410 (2017).

[7] T. Eto, M. Ishizuka, S. Endo, T. Kanomata, and T. Kikegawa, "Pressure-induced structural phase transition in a ferromagnet CrTe," J Alloys Compd **315**(1), 16–21 (2001).

[8] N. Abuawwad, M. dos Santos Dias, H. Abusara, and S. Lounis, "Noncollinear magnetism in two-dimensional CrTe2," Journal of Physics: Condensed Matter **34**(45), 454001 (2022).

[9] X. Zhang, Q. Lu, W. Liu, W. Niu, J. Sun, J. Cook, M. Vaninger, P.F. Miceli, D.J. Singh, S.-W. Lian, T.-R. Chang, X. He, J. Du, L. He, R. Zhang, G. Bian, and Y. Xu, "Room-temperature intrinsic ferromagnetism in epitaxial CrTe2 ultrathin films," Nat Commun **12**(1), 2492 (2021).

[10] D.C. Freitas, R. Weht, A. Sulpice, G. Remenyi, P. Strobel, F. Gay, J. Marcus, and M. Núñez-Regueiro, "Ferromagnetism in layered metastable 1T-CrTe2," Journal of Physics: Condensed Matter **27**(17), 176002 (2015).

[11] F. Wang, J. Du, F. Sun, R.F. Sabirianov, N. Al-Aqtash, D. Sengupta, H. Zeng, and X. Xu, "Ferromagnetic Cr2Te3 nanorods with ultrahigh coercivity," Nanoscale **10**(23), 11028–11033 (2018).

[12] S.J. Youn, S.K. Kwon, and B.I. Min, "Correlation effect and magnetic moments in Cr2Te3," J Appl Phys **101**(9), 09G522 (2007).

[13] T. Hashimoto, K. Hoya, M. Yamaguchi, and I. Ichitsubo, "Magnetic Properties of Single Crystals Cr2-δTe3," J Physical Soc Japan **31**(3), 679–682 (1971).

[14] E.F. Bertaut, G. Roult, R. Aleonard, R. Pauthenet, M. Chevreton, and R. Jansen, "Structures magnétiques de Cr3X4 (X = S, Se, Te)," J. Phys. France **25**(5), 582–595 (1964).

[15] M. Yamaguchi, and T. Hashimoto, “Magnetic Properties of Cr3Te4 in Ferromagnetic Region,” J Physical Soc Japan **32**, 635–638 (1972).

[16] K. Yaji, A. Kimura, C. Hirai, M. Taniguchi, M. Koyama, H. Sato, K. Shimada, A. Tanaka, T. Muro, S. Imada, and S. Suga, “Electronic structure of ${\mathrm{Cr}}_{1\text{\penalty1000-\hskip0pt}\ensuremath{\delta}}X(X=\mathrm{S},\mathrm{Te})$ studied by Cr $2p$ soft x-ray magnetic circular dichroism,” Phys Rev B **70**(6), 64402 (2004).

[17] Y. Liu, M. Abeykoon, E. Stavitski, K. Attenkofer, and C. Petrovic, “Magnetic anisotropy and entropy change in trigonal ${\mathrm{Cr}}_{5}{\mathrm{Te}}_{8}$,” Phys Rev B **100**(24), 245114 (2019).

[18] X. Zhang, T. Yu, Q. Xue, M. Lei, and R. Jiao, “Critical behavior and magnetocaloric effect in monoclinic Cr5Te8,” J Alloys Compd **750**, 798–803 (2018).

[19] R. Mondal, R. Kulkarni, and A. Thamizhavel, “Anisotropic magnetic properties and critical behaviour studies of trigonal Cr5Te8 single crystal,” J Magn Magn Mater **483**, 27–33 (2019).

[20] K. Lukoschus, S. Kraschinski, C. Näther, W. Bensch, and R.K. Kremer, “Magnetic properties and low temperature X-ray studies of the weak ferromagnetic monoclinic and trigonal chromium tellurides Cr5Te8,” J Solid State Chem **177**(3), 951–959 (2004).

[21] A.F. Andresen, S.E. Rasmussen, E.L. Hirvisalo, and J. Munch-Petersen, “A NEUTRON DIFFRACTION INVESTIGATION OF Cr$sub 2$Te$sub 3$ AND Cr$sub 5$Te$sub 6$,” Acta Chem Scand **17**, 1335–1342 (1963).

[22] J Dijkstra, H H Weitering, C F van Bruggen, C Haas, and R A de Groot, “Band-structure calculations, and magnetic and transport properties of ferromagnetic chromium tellurides (CrTe, Cr3Te4, Cr2Te3),” Journal of Physics: Condensed Matter **1**(46), 9141 (1989).

[23] F. Grønvold, and E.F. Westrum Jr., “Thermodynamic aspects of the magnetic transitions in the chromium tellurides Heat Capacities of Cr5Te6, Cr3Te4 and Cr2Te3 from 5 to 350°K,” Z Anorg Allg Chem **328**(5–6), 272–282 (1964).

[24] K. Sato, Y. Aman, M. Hirai, and M. Fujisawa, “Reflectivity Spectra in Single Crystals of Cr3Te4, Cr2Te3 and Cr2Se3 between 0.3 and 23 eV,” J Physical Soc Japan **59**(2), 435–438 (1990).

[25] T. Hirone, and S. Chiba, “On the Magnetic Anisotropy of Single Crystal of Chromium Telluride,” J Physical Soc Japan **15**(11), 1991–1994 (1960).

[26] K. Yaji, A. Kimura, M. Koyama, C. Hirai, H. Sato, K. Shimada, A. Tanaka, and M. Taniguchi, “Soft x-ray magnetic circular dichroism study of Cr tellurides,” J Appl Phys **97**(10), 10A316 (2005).

[27] R. Saha, H.L. Meyerheim, B. Göbel, B.K. Hazra, H. Deniz, K. Mohseni, V. Antonov, A. Ernst, D. Knyazev, A. Bedoya-Pinto, I. Mertig, and S.S.P. Parkin, “Observation of Néel-type skyrmions in acentric self-intercalated Cr1+δTe2,” Nat Commun **13**(1), 3965 (2022).

[28] A. Purbawati, J. Coraux, J. Vogel, A. Hadj-Azzem, N. Wu, N. Bendiab, D. Jegouso, J. Renard, L. Marty, V. Bouchiat, A. Sulpice, L. Aballe, M. Foerster, F. Genuzio, A. Locatelli, T.O. Menteş, Z.V. Han, X. Sun, M. Núñez-Regueiro, and N. Rougemaille, “In-Plane Magnetic Domains and Néel-like

Domain Walls in Thin Flakes of the Room Temperature CrTe2 Van der Waals Ferromagnet," ACS Appl Mater Interfaces **12**(27), 30702–30710 (2020).

[29] L. Meng, Z. Zhou, M. Xu, S. Yang, K. Si, L. Liu, X. Wang, H. Jiang, B. Li, P. Qin, P. Zhang, J. Wang, Z. Liu, P. Tang, Y. Ye, W. Zhou, L. Bao, H.-J. Gao, and Y. Gong, "Anomalous thickness dependence of Curie temperature in air-stable two-dimensional ferromagnetic 1T-CrTe2 grown by chemical vapor deposition," Nat Commun **12**(1), 809 (2021).

[30] Y. Ou, W. Yanez, R. Xiao, M. Stanley, S. Ghosh, B. Zheng, W. Jiang, Y.-S. Huang, T. Pillsbury, A. Richardella, C. Liu, T. Low, V.H. Crespi, K.A. Mkhoyan, and N. Samarth, "ZrTe2/CrTe2: an epitaxial van der Waals platform for spintronics," Nat Commun **13**(1), 2972 (2022).

[31] V. Franco, and A. Conde, "Scaling laws for the magnetocaloric effect in second order phase transitions: From physics to applications for the characterization of materials," International Journal of Refrigeration **33**(3), 465–473 (2010).

[32] L.-Z. Zhang, A.-L. Zhang, X.-D. He, X.-W. Ben, Q.-L. Xiao, W.-L. Lu, F. Chen, Z. Feng, S. Cao, J. Zhang, and J.-Y. Ge, "Critical behavior and magnetocaloric effect of the quasi-two-dimensional room-temperature ferromagnet $\mathrm{Cr}{}_{4}\mathrm{Te}{}_{5}$," Phys Rev B **101**(21), 214413 (2020).

[33] A. Goswami, N. Ng, E. Yakubu, A.M.M. Abeykoon, and S. Guchhait, "Critical behavior in monoclinic ${\mathrm{Cr}}_{3}{\mathrm{Te}}_{4}$," Phys Rev B **109**(5), 54413 (2024).

[34] L.-Z. Zhang, Q.-L. Xiao, F. Chen, Z. Feng, S. Cao, J. Zhang, and J.-Y. Ge, "Multiple magnetic phase transitions and critical behavior in single crystal Cr5Te6," J Magn Magn Mater **546**, 168770 (2022).

[35] G.M. Sheldrick, "Crystal structure refinement with SHELXL," Acta Crystallographica Section C **71**(1), 3–8 (2015).

[36] R.C. Clark, and J.S. Reid, "The analytical calculation of absorption in multifaceted crystals," Acta Crystallographica Section A **51**(6), 887–897 (1995).

[37] A.F. Andresen, E. Zeppezauer, T. Boive, B. Nordström, and C.I. Brändén, "The Magnetic Structure of Cr2Te3, Cr3Te4, and Cr5Te6.," Acta Chem Scand **24**, 3495–3509 (1970).

[38] C.-K. Tian, C. Wang, W. Ji, J.-C. Wang, T.-L. Xia, L. Wang, J.-J. Liu, H.-X. Zhang, and P. Cheng, "Domain wall pinning and hard magnetic phase in Co-doped bulk single crystalline ${\mathrm{Fe}}_{3}{\mathrm{GeTe}}_{2}$," Phys Rev B **99**(18), 184428 (2019).

[39] T. Moriya, "Theory of itinerant electron magnetism," J Magn Magn Mater **100**(1), 261–271 (1991).

[40] E.P. Wohlfarth, "Magnetic properties of crystallineand amorphous alloys: A systematic discussion based on the Rhodes-Wohlfarth plot," J Magn Magn Mater **7**(1), 113–120 (1978).

[41] Y. Liu, and C. Petrovic, "Critical behavior and magnetocaloric effect in ${\mathrm{Mn}}_{3}{\mathrm{Si}}_{2}{\mathrm{Te}}_{6}$," Phys Rev B **98**(6), 64423 (2018).

[42] Y. Liu, and C. Petrovic, "Critical behavior of quasi-two-dimensional semiconducting ferromagnet ${\mathrm{Cr}}_{2}{\mathrm{Ge}}_{2}{\mathrm{Te}}_{6}$," Phys Rev B **96**(5), 54406 (2017).

[43] W. Liu, Y. Dai, Y.-E. Yang, J. Fan, L. Pi, L. Zhang, and Y. Zhang, “Critical behavior of the single-crystalline van der Waals bonded ferromagnet ${\mathrm{Cr}}_{2}{\mathrm{Ge}}_{2}{\mathrm{Te}}_{6}$,” Phys Rev B **98**(21), 214420 (2018).

[44] A. Arrott, “Criterion for Ferromagnetism from Observations of Magnetic Isotherms,” Physical Review **108**(6), 1394–1396 (1957).

[45] A. Arrott, and J.E. Noakes, “Approximate Equation of State For Nickel Near its Critical Temperature,” Phys Rev Lett **19**(14), 786–789 (1967).

[46] B. Banerjee, “On a generalised approach to first and second order magnetic transitions,” Physics Letters **12**, 16–17 (1964).

[47] S.N. Kaul, “Static critical phenomena in ferromagnets with quenched disorder,” J Magn Magn Mater **53**(1), 5–53 (1985).

[48] H. E. Stanley, *Introduction to Phase Transition and Critical Phenomena* (Oxford University press, 1971).

[49] M E Fisher, “The theory of equilibrium critical phenomena,” Reports on Progress in Physics **30**(2), 615 (1967).

[50] A.K. Pramanik, and A. Banerjee, “Critical behavior at paramagnetic to ferromagnetic phase transition in ${\text{Pr}}_{0.5}{\text{Sr}}_{0.5}{\text{MnO}}_{3}$: A bulk magnetization study,” Phys Rev B **79**(21), 214426 (2009).

[51] J.S. Kouvel, and M.E. Fisher, “Detailed Magnetic Behavior of Nickel Near its Curie Point,” Physical Review **136**(6A), A1626–A1632 (1964).

[52] B. Widom, “Equation of State in the Neighborhood of the Critical Point,” J Chem Phys **43**(11), 3898–3905 (2004).

[53] A. Taroni, S.T. Bramwell, and P.C.W. Holdsworth, “Universal window for two-dimensional critical exponents,” Journal of Physics: Condensed Matter **20**(27), 275233 (2008).

[54] M.E. Fisher, S. Ma, and B.G. Nickel, “Critical Exponents for Long-Range Interactions,” Phys Rev Lett **29**(14), 917–920 (1972).

[55] S.F. Fischer, S.N. Kaul, and H. Kronmüller, “Critical magnetic properties of disordered polycrystalline ${\mathrm{Cr}}_{75}{\mathrm{Fe}}_{25}$ and ${\mathrm{Cr}}_{70}{\mathrm{Fe}}_{30}$ alloys,” Phys Rev B **65**(6), 64443 (2002).